AVO inversion of multicomponent data for P and S impedance

Faranak Mahmoudian and Gary F. Margrave

ABSTRACT

Procedures to invert P-P and P-S prestack seismic data for underlying compressional and shear wave impedance reflectivity have been developed in the past. A program has been written to perform a joint AVO inversion on PP and PS pre-stack synthetic data in MATLAB. The inversion can be done for pure compressional wave (PP), as well as only converted shear wave (PS data) resulting in PP inversion only and PS inversion only. The program is primarily intended to perform an AVO inversion utilizing a model-based, weighted stacking approach similar to established PP and joint inversion methods. Missing low-frequency components in seismic datasets cause low-cut filtered reflectivity in the inversion process. The inversion program is organized to provide missing low-frequency components of impedance from well log information. The inverted impedance reflectivity results from PP, PS only inversion and joint inversion are compared using synthetic noise-free data. In the noise-free case all three methods have similar performance. In presence of noise, the joint inversion method performs significantly better than the results of PP and PS inversion only.

INTRODUCTION

The variation of reflection and transmission coefficients with incident angle, and thus offset, is commonly known as offset-dependent reflectivity, or amplitude versus offset (AVO). The Zoeppritz equations describe the reflection and transmission coefficients as a function of incident angle and elastic media properties (density, P-wave velocity, and S-wave velocity). Since the Zoeppritz equations are highly nonlinear with respect to velocities and density, many approximations have been made in order to linearize them. Aki and Richards (1980) assumed small layer contrasts and simplified these equations. Linear approximations for PP and PS reflection coefficients, R_{PP} and $R_{PS,}$ can be reformulated as function of P-wave (I), and S-wave impedance (J) (Larsen 1999). In this case $I = \alpha\rho, (\Delta I/I = \Delta\alpha/\alpha + \Delta\rho/\rho)$ and $J = \beta\rho, \ (\Delta J/J = \Delta\beta/\beta + \Delta\rho/\rho)$, where α, β and ρ are the average P-wave, S-wave and density values across an interface, respectively and:

$$R_{PP}(\theta) \approx \frac{(1+\tan^2\theta)}{2}\frac{\Delta \mathrm{I}}{\mathrm{I}} - 4\frac{\beta^2}{\alpha^2}\sin^2\theta\frac{\Delta \mathrm{J}}{\mathrm{J}} - \left[\frac{1}{2}\tan^2\theta - 2\frac{\beta^2}{\alpha^2}\sin^2\theta\right]\frac{\Delta\rho}{\rho}. \qquad (1a)$$

$$R_{PS}(\theta,\phi) \approx -\frac{\alpha\tan\varphi}{2\beta}\left[\left(1+2\sin^2\varphi - \frac{2\beta}{\alpha}\cos\theta\cos\varphi\right)\frac{\Delta\rho}{\rho} - \left(4\sin^2\varphi - \frac{4\beta}{\alpha}\cos\theta\cos\varphi\right)\frac{\Delta \mathrm{J}}{\mathrm{J}}\right]. \qquad (1b)$$

In the above equations, θ is the average of the P-wave angle of incidence and transmission across the interface, and φ is the average of the shear-wave angle of reflection and transmission across the interface.

Using Gardner's relation $\rho \approx \alpha^{1/4}$, the density contrast term can be rewritten as a function of P-wave impedance, $\frac{\Delta\rho}{\rho} = \frac{1}{5}\frac{\Delta I}{I}$. Applying this assumption, Larson (1999) rewrites the Aki and Richards (equations 1-a and 1-b)as:

$$\left.\begin{aligned} R_{PP}(\theta_P) &= A(\theta_P)\frac{\Delta I}{I} + B(\theta_P)\frac{\Delta J}{J} \\ R_{PS}(\theta_S,\varphi_S) &= C(\theta_S,\varphi_S)\frac{\Delta I}{I} + D(\theta_S,\varphi_S)\frac{\Delta J}{J} \end{aligned}\right\} \qquad (2)$$

where

$$\left.\begin{aligned} \mathrm{A}(\theta_P) &= \frac{(1+\tan^2\theta_P)}{2} \\ B(\theta_P) &= -4\frac{\beta^2}{\alpha^2}\sin^2\theta_P \\ C(\theta_S,\varphi_S) &= \frac{-\alpha\tan\varphi_S}{10\beta}\left(1+2\sin^2\varphi_S - 2\frac{\beta}{\alpha}\cos\theta_S\cos\varphi_S\right) \\ D(\theta_S,\varphi_S) &= \frac{\alpha\tan\varphi_S}{\beta}\left(2\sin^2\varphi_S - 2\frac{\beta}{\alpha}\cos\theta_S\cos\varphi_S\right) \end{aligned}\right\} \qquad (3)$$

The coefficients A, B, C, and D are functions of the angle θ_P (the average of P-wave incident, and transmission angle) for the PP section, and angle θ_S (the average of P-wave incident and transmission angle) and the angle φ_S (the average of the S-wave reflection and transmission angle) for the PS section and the β/α of the model (rather than of the

data itself). Figure 1 shows the θ_P , θ_S and φ_S for a set of source-receiver. Note that θ_P and θ_S are different given the same source-receiver offset.

$$\theta_P = \frac{\theta_{1P} + \theta_{2P}}{2} \quad \theta_S = \frac{\theta_{1S} + \theta_{2S}}{2} \quad \varphi_S = \frac{\varphi_{1S} + \varphi_{2S}}{2}$$

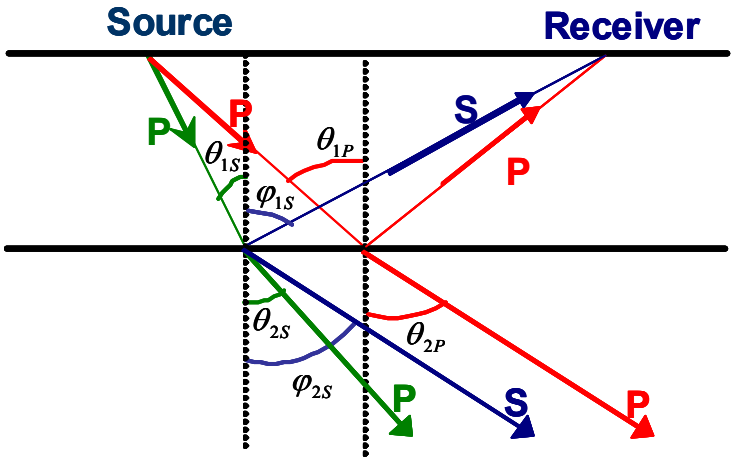

FIG 1. Raypath geometry for pure compressional (P-P) and converted wave (P-S)

JOINT LEAST-SQUARES INVERSION

Smith and Gidlow (1987) showed that the Aki and Richards approximation for R_{PP} (equation 1a) can be inverted (by least-square inversion of PP data) for $\Delta\alpha/\alpha$ and $\Delta\beta/\beta$ in the form of a weighted stacking scheme. Also, Stewart (1990) derived the extension of the Smith-Gidlow approach using both PP and PS reflections to constrain $\Delta\alpha/\alpha$ and $\Delta\beta/\beta$. Larsen (1999) outlined a least-square, weighted-stacking procedure incorporating both PP and PS seismic data to extract P-wave impedance reflectivity $\Delta I/I$ and S-wave impedance reflectivity $\Delta J/J$. In this method, normal-moveout (NMO) corrected common-mid point (CMP) (PP case) and common conversion point (CCP) (PS case) gathers are weighted and stacked. The weights are derived from a smoothed background velocity model. If N is the number of offsets contributing to each NMO corrected CMP or CCP gather at a particular time sample under consideration, the stacking weights for estimating the $\Delta I/I$ and $\Delta J/J$ (Larsen, 1999) are given by:

$$\begin{aligned}
\Delta I/I &= \sum_{\text{k=offset}} wtsppI(\theta_{P_k}, \theta_{S_k}, \varphi_{S_k})\, \mathrm{R}_{\mathrm{PP}}(\theta_{P_k}) + \sum_{\text{k=offset}} wtspsI(\theta_{P_k}, \theta_{S_k}, \varphi_{S_k})\, \mathrm{R}_{\mathrm{PS}}(\theta_{S_k}, \varphi_{S_k}) \\
\Delta J/J &= \sum_{\text{k=offset}} wtsppJ(\theta_{P_k}, \theta_{S_k}, \varphi_{S_k})\, \mathrm{R}_{\mathrm{PP}}(\theta_{P_k}) + \sum_{\text{k=offset}} wtspsJ(\theta_{P_k}, \theta_{S_k}, \varphi_{S_k})\, \mathrm{R}_{\mathrm{PS}}(\theta_{S_k}, \varphi_{S_k})
\end{aligned} \tag{4}$$

where, as before, the angle θ_P is the average of P-wave incident and transmission angle in the PP section, the angle θ_S is the average of P-wave incident and transmission angle in PS section and the angle φ_S is the average of S-wave reflection and transmission angle

in PS section, respectively, for the k^{th} offset. The (wtsppI , wtsppJ) and (wtspsI , wtspsJ) are the stacking weights for the PP and PS reflection data respectively, and are given by:

$$\text{wtsppI} = \frac{\left(A_i \sum_{i=1}^{N} (B_i^2 + D_i^2) - B_i \sum_{i=1}^{N} (A_i B_i + C_i D_i) \right)}{\sum_{i=1}^{N} (A_i^2 + C_i^2) \sum_{i=1}^{N} (B_i^2 + D_i^2) - \left[\sum_{i=1}^{N} (A_i B_i + C_i D_i) \right]^2}$$

$$\text{wtspsI} = \frac{\left(C_i \sum_{i=1}^{N} (B_i^2 + D_i^2) - D_i \sum_{i=1}^{N} (A_i B_i + C_i D_i) \right)}{\sum_{i=1}^{N} (A_i^2 + C_i^2) \sum_{i=1}^{N} (B_i^2 + D_i^2) - \left[\sum_{i=1}^{N} (A_i B_i + C_i D_i) \right]^2} \qquad (5)$$

$$\text{wtsppJ} = \frac{\left(B_i \sum_{i=1}^{N} (A_i^2 + C_i^2) - A_i \sum_{i=1}^{N} (A_i B_i + C_i D_i) \right)}{\sum_{i=1}^{N} (A_i^2 + C_i^2) \sum_{i=1}^{N} (B_i^2 + D_i^2) - \left[\sum_{i=1}^{N} (A_i B_i + C_i D_i) \right]^2}$$

$$\text{wtspsJ} = \frac{\left(D_i \sum_{i=1}^{N} (A_i^2 + C_i^2) - C_i \sum_{i=1}^{N} (A_i B_i + C_i D_i) \right)}{\sum_{i=1}^{N} (A_i^2 + C_i^2) \sum_{i=1}^{N} (B_i^2 + D_i^2) - \left[\sum_{i=1}^{N} (A_i B_i + C_i D_i) \right]^2} \qquad (6)$$

Equation (4) is the equation that has been coded in MATLAB to invert the reflection amplitudes to P-wave impedance reflectivity $\Delta I/I$ and S-wave impedance reflectivity $\Delta J/J$.

IMPLEMENTATION OF LEAST SQUARES INVERSION

The joint inversion program is designed to have a PP and a PS synthetic section, as well as a velocity-depth model as input. The inversion program uses the 'mudrock line' of Castagna et al. (1985) to obtain the S-wave velocity model from P-wave velocity, wherever *Vs* log is not available. Additionally, PP data or PS data alone can be used as input, resulting in a PP inversion only or PS inversion only, respectively. The joint inversion program works with the PP and PS synthetics as built in SYNTH software (a routine in CREWES MATLAB library). The PP and PS synthetics created in SYNTH have reflection amplitudes computed with the exact Zoeppritz equations. This implementation computes primaries only (no multiples), does not include transmission losses or spherical spreading. As well, NMO is removed; but moveout stretch effects are present. The synthetic PP and PS sections are in time. Both seismograms were created initially as broad-band responses and then convolved with the appropriate wavelet. Figure 2 shows an example of PP and PS synthetics for a simple log model, in which both the PP and PS seismograms have an initial 10-80 Hz zero-phase (Butterworth) wavelet and the

same offset range from 0 to 1000 m. In Figure 2, three reflection events base on the log model (Figure 2a), can be recognized easily in both PP and PS synthetics.

The combination of PP and PS data in an inversion requires that the two data types be correlated in time or depth. We followed a procedure to correlate the PP and PS synthetic sections in depth. The PP and PS synthetics were converted to depth using the SEIS2Z routine, developed in MATLAB. SEIS2Z converts input synthetics from time to depth using a time-depth curve. We created separate time-depth curves for PP and PS using our well logs. Accurate depth conversion properly correlates the events on the PP and PS sections. Figure 3 shows the PP and PS synthetics, derived from the simple logs model (Figure 2a), in depth.

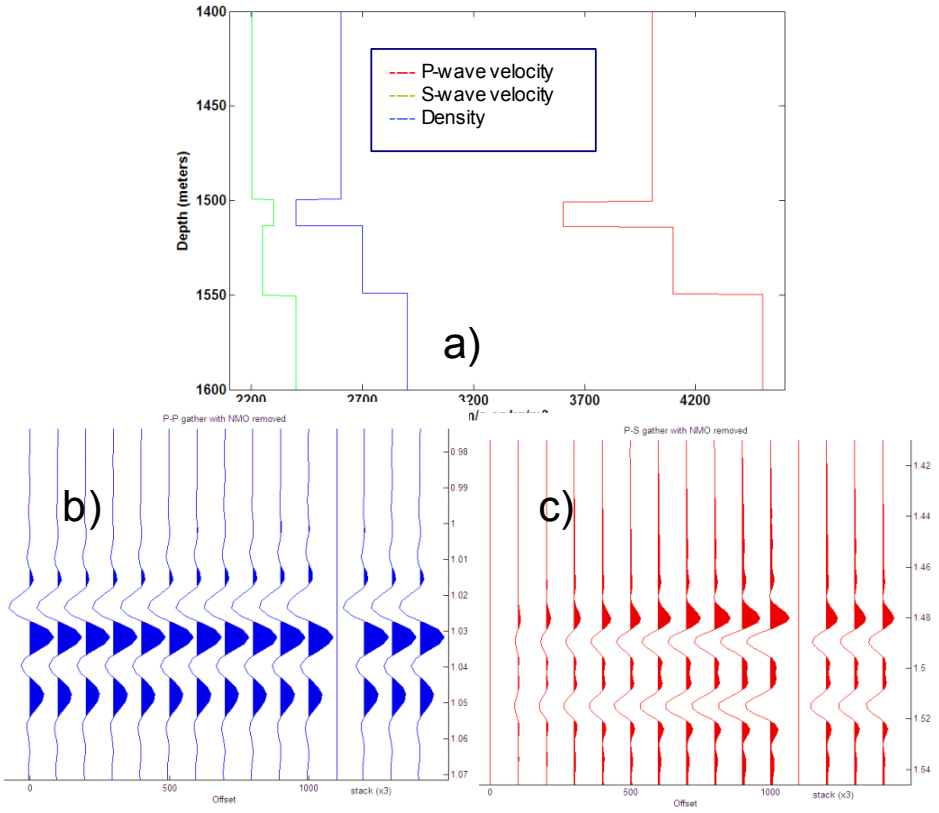

FIG. 2. (a) A simple log model in depth. In this plot the density log added by constant value of 400 for better display. (b) A synthetic CMP gather from the model in Figure 2a, in PP time. (c) A synthetic CCP gather from the model in Figure 2a, in PS time. In each seismogram, the three traces on the right are three repetitions of the stacked trace. Both seismograms have the initial Butterworth wavelet

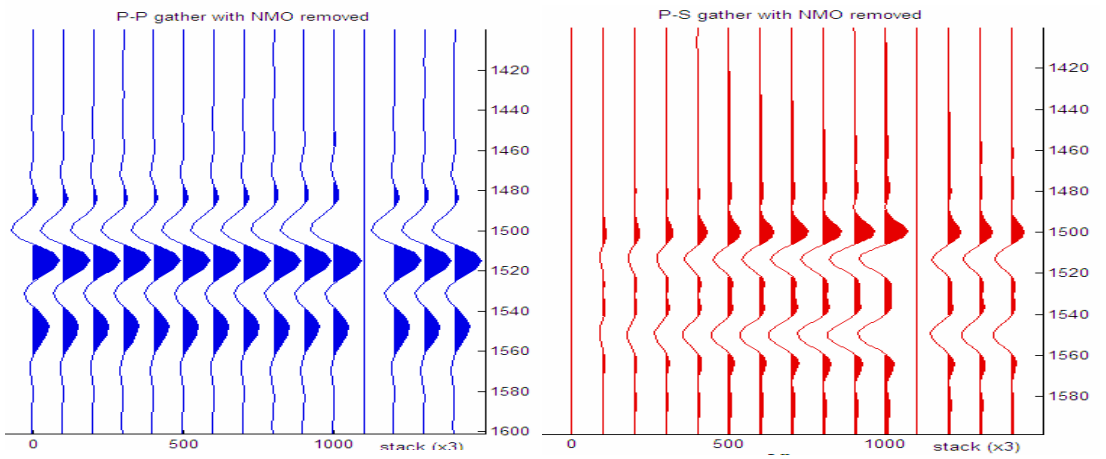

FIG. 3. The PP (blue) and PS (red) synthetic gathers after conversion to depth. The required θ_P, θ_S and φ_S in a depth sample and second offset is shown as an example.

Using equations (5) and (6), the stacking weights for the PP and PS synthetics were computed using the coefficients A, B, C and D in equation (3). The incident and reflection angles θ_P, θ_S and φ_S are determined by raytracing on a smooth background velocity model. The angle θ_P at each depth sample and offset in the PP section was computed by TRACERAY_PP, (a MATLAB raytracing routine for PP sections, CREWES MATLAB library), also the angle θ_S and φ_S at each depth sample and offset was computed by TRACERAY_PS, (a MATLAB raytracing routine for PS sections, CEREWES MATLAB library).

The β/α ratio, required for computing the coefficients of equation (3), is obtained by strongly smoothing the input velocities. If an S-wave velocity is not available, the joint inversion program uses the mudrock line to calculate the S-wave velocity log. After calculating the stacking weights for each depth sample, the weights are multiplied by R_{PP} and R_{PS}, the reflection amplitude of each synthetic as mentioned in equation (4). Then the impedance reflectivity results, $\Delta I/I$ and $\Delta J/J$ are estimated for each depth sample. The stacking weights required to estimate $\Delta I/I$ and $\Delta J/J$ for the logs model in Figure 2a, are shown in Figures 4 and 5, respectively.

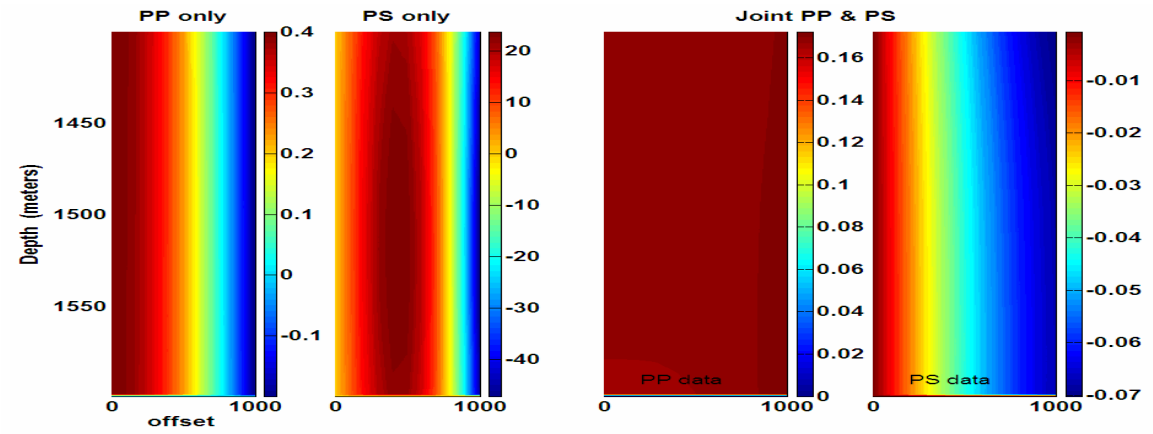

FIG. 4. The stacking weights required to estimate ΔI/I in PP inversion only (left) and PS inversion only (middle) and joint inversion (right), for the log model in Figure 2a. The joint method needs two sets of weights, for PP and PS data. Note the colour bars on the right of each plot.

The weights for joint inversion in estimation of $\Delta I/I$, the PS weights are very small compared to weights applied to the PP section, Figure 3. Thus in joint version, PS data have a smaller influence on $\Delta I/I$ estimation than do PP data. For $\Delta J/J$ estimation in joint inversion, the PP weights are small compared to the PS weights (Figure 4), thus PS data dominates the$\Delta J/J$ estimation in joint inversion.

Further examination of the stacking weights for estimation of $\Delta I/I$ in Figure 4 and for the $\Delta J/J$ in Figure 5, reveals that the joint inversion stacking weights have the highest value in PP and PS data where there is high amplitude. It appears that the result for $\Delta I/I$ and $\Delta J/J$ could be significantly improved by the joint inversion method. For impedance estimation using Aki and Richards polarity convention, the PS reflection (in land data) has negative while PP reflection has positive amplitude. That is why the highest magnitude weights for PS data in joint inversion are negative in Figures 4-5.

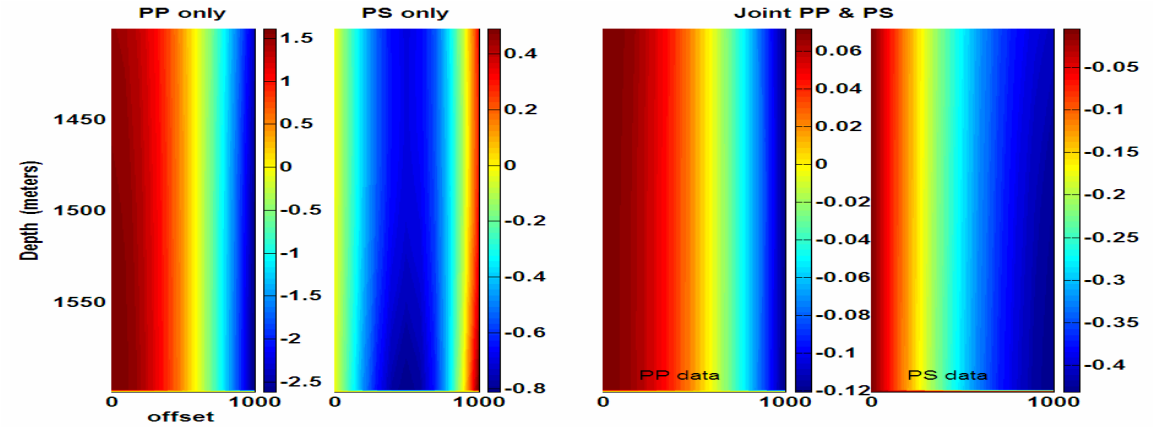

FIG. 5. The stacking weights required to estimate ΔJ/J in PP inversion only (left) and PS inversion only (middle) and joint PP and PS method (right), for the log model in Figure 2a. The joint method needs two sets of weights, for PP and PS data. Note the color bars on the right of each plot.

For the joint inversion, the PS data is examined with SEG polarity convention. Using the reverse polarity, the $\Delta I/I$ estimation didn't change, however; for the $\Delta J/J$ estimation, on which the PS data dominates, the result was reversed. Moreover, it is predictable by the weights (Figures 4 and 5).

The $\Delta I/I$ and $\Delta J/J$ as estimated from PP, PS only and joint inversion of the log model in Figure 2a, are shown in Figures 6 and 7, respectively. In Figures 6 and 7, the depth of each reflector is adequately determined, but the magnitude of $\Delta I/I$ and $\Delta J/J$ has a scaling problem that is due to the scaling factor used in generating the synthetics. With true seismic sections, the lack of true amplitude in the data processing would cause a similar difference. This scaling effect is minimized after the low-frequency content is restored.

Looking at Figure 6, it seems that only the PS inversion does not produce a good estimate of $\Delta I/I$, while the PP-only and joint-inversion produce nearly identical estimates of $\Delta I/I$. In the next sections we will show that after restoration of low frequency, the estimate of $\Delta I/I$ from all three methods are almost identical. In Figures 6 and 7 the estimated $\Delta I/I$ and $\Delta J/J$ are not ideal spikes. This is because the seismic data are band-limited. In Figures 6 and 7 the blue curves are true P-wave and S-wave reflectivity calculated from the logs, multiplied by a scalar factor so that a comparison can be made. This scalar factor is the magnitude of the initial wavelet peak.

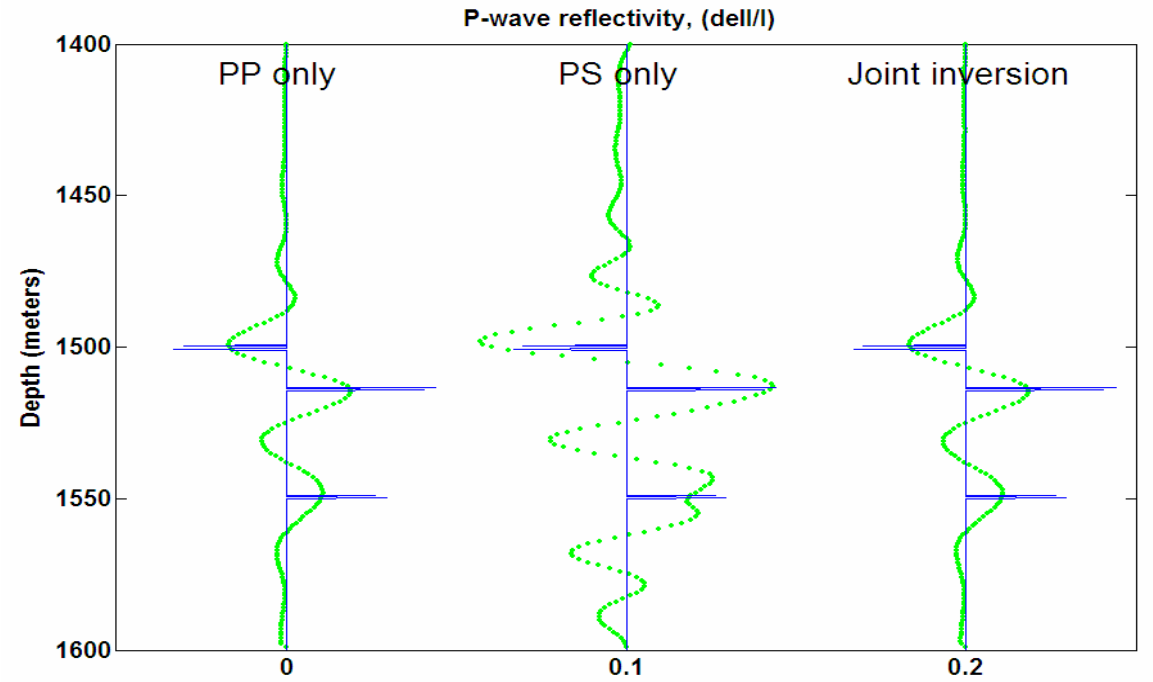

FIG. 6. (ΔI/I) as estimated from PP inversion only (left), PS inversion only (middle) and joint inversion (right), for the log model in Figure 2a. In each plot, the green curve is ΔI/I calculated by code and the blue curve is the real ΔI/I calculated directly from the model log of Figure 2a.

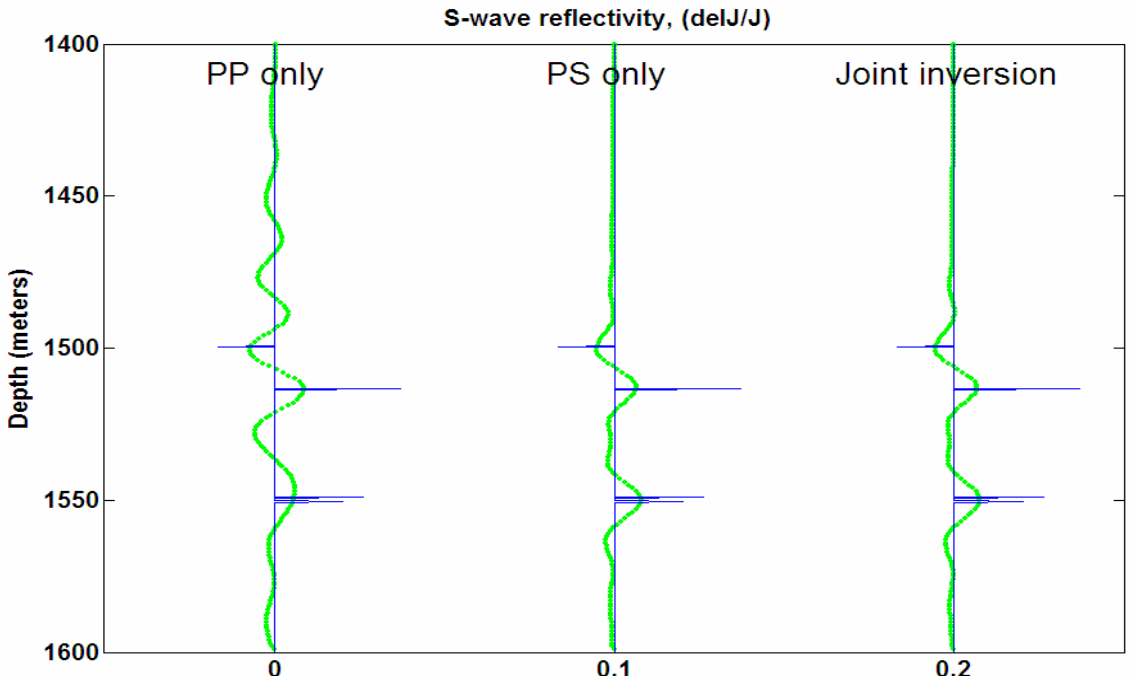

FIG. 7. (ΔJ/J) as estimated from PP inversion only (left), PS inversion only (middle), and joint inversion (right), for the log model in Figure 2a. In each plot, the green curve is ΔJ/J calculated by code and the blue curve is the real ΔI/I calculated directly from the model log of Figure 2a.

INVERSION OF BAND-LIMITED DATA

Missing low-frequency components is a common effect in seismic data. The main reason is due to band-limited seismic sources and using band-pass filters in data processing. Band-pass filters usually apply to data in the frequency domain to eliminate the low-frequency ground-roll waves or some coherent high frequency noise. In this process also some desired low-frequency data is missing. Inversion of such band-limited data would result in band-limited impedance. Lindseth (1979) stated that the inversion of the reflection coefficient leads to band-limited velocity coefficients (impedance logs). Figure 8a, illustrates the effect of missing low-frequency components of a sonic log, which evidently contain much of the essential velocity information. Without low-frequency components, the synthetic sonic log values obtained from inverting seismic data do not closely approximate velocities measured on borehole sonic logs. The moderately high-frequency reflection components are recoverable by proper acquisition and data processing; the very low frequencies, representing the gross velocity information, must be obtained elsewhere. Removal of the high-frequency components of seismic data results in decreases resolution (Lindseth 1979), as shown in Figure 8b. Borehole logs are used to extend such band-limited impedance into regions of the estimated log spectrum. Lindseth (1979) used the reflection-derived velocity analyses or sonic log data to recover the missing low-frequency components.

Waters (1987) described an inversion scheme to estimate impedance values from PP seismic data, while preserving the low-frequency content. Ferguson and Margrave (1996) extended Water's (1978) method to a band-limited impedance inversion which has been implemented as a MATLAB algorithm, called BLIMP (band-limited impedance

inversion). To restore low-frequency trends to joint inversion or PP only or PS inversion only results, an impedance estimate derived from well logs or stacking velocities is used.

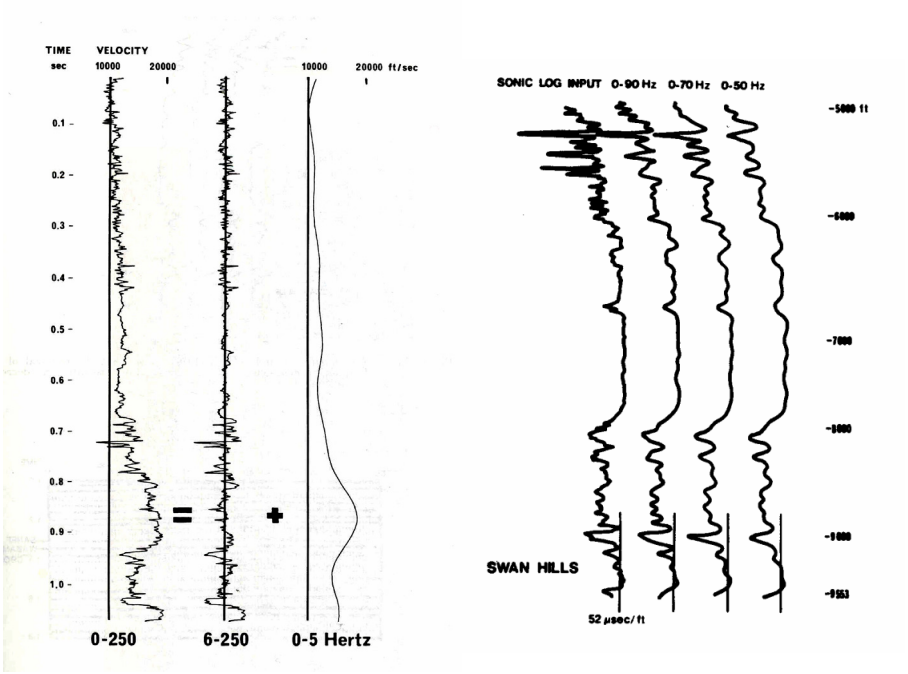

a) b)

FIG. 8. (a) A sonic log may be considered to be the sum of a gross velocity function (0-5 HZ) and a detailed velocity function (6-250 HZ), after Lindseth (1979). (b) Removing successively increasing amounts of high-frequency components from sonic logs correspondingly results in decreased resolution, after Lindseth (1979).

LOW-FREQUENCY COMPENSATION

The Band-Limited Impedance routine (BLIMP, found in CREWES MATLAB library), uses impedance estimated from log model to provide the missing low-frequency components of input seismic data. Briefly, the linear trend of true impedance is computed and subtracted from the impedance estimated itself. Then the low-frequency components of the true impedance are selected by applying a low-cut filter to its amplitude spectrum. The result is added to the amplitude spectrum of the impedance computed by the inversion code. After taking the inverse Fourier transform of the impedance and adding the linear trend to that, the result is impedance with restored low-frequency components. The following is a step-by-step description of the BLIMP method (Ferguson and Margrave, 1996):

1) Compute the linear trend of the true impedance estimated from sonic logs.

2) Subtract the linear trend from true impedance estimated.

3) Compute the Fourier spectrum of step (2).

4) Compute the Fourier spectrum of reflectivity (ΔI/I and ΔJ/J, computed from the inversion code).

5) Determine a scalar to match the mean magnitude of (4) and (3) over the seismic signal band.

6) Multiply the spectra of (4) by the scalar from (5)

7) Low-pass filter (3) and add to (6).

8) Inverse Fourier transform (7).

9) Add the –frequency trend from (1) to (8).

The joint inversion program uses an impedance estimate, derived from well-logs to provide the low-frequency components commonly missing in seismic data, required by the BLIMP routine.

INVERSION RESULTS AFTER APPLYING BLIMP

The joint inversion program as mentioned before, has been used to convert the PP and PS synthetics depth. Thus the frequency content of these data are described by k_Z, the spatial frequency. The Minimum and Maximum of k_z required for restoring the low frequency components is input by the user. The amplitude spectrum of the PP and PS data, show the frequency content is similar to that of the initial wavelet, as expected by convolution theory, and the assumption of white reflectivity. Thus, to determine the required minimum and maximum frequency (k_Z) required by BLIMP, the frequency spectrum of initial wavelet was examined. A schematic algorithm of joint inversion program to restore the low-frequency content is shown in Figure 9.

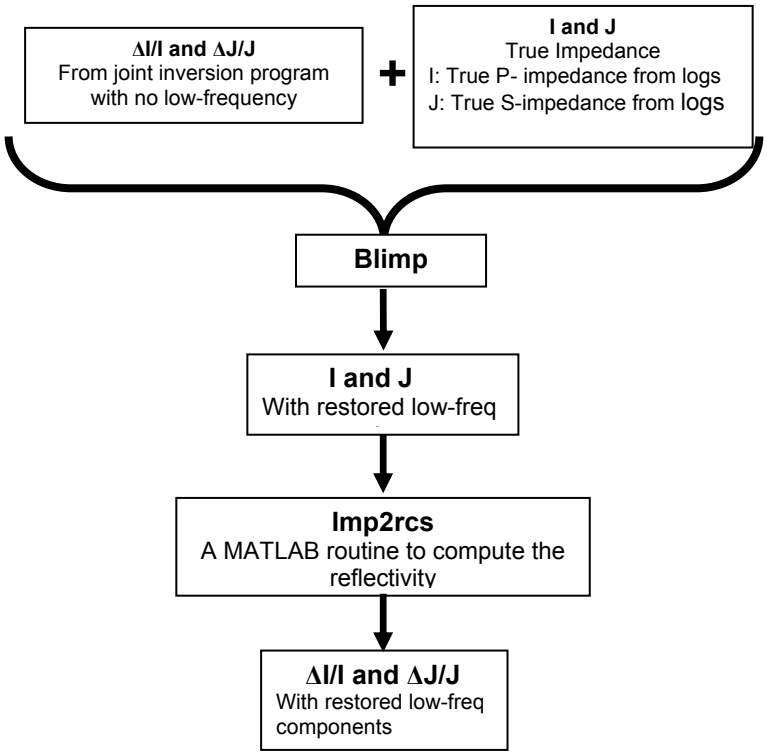

FIG. 9. A schematic algorithm explaining the procedure of restoring the low-frequency components to ΔI/I and ΔJ/J in the inversion code.

If the input seismic data are narrow-band (e.g. 20-100 Hz) BLIMP significantly improves the impedance estimate (see Figures 13-14). For broader band data the influence of BLIMP is less important, but nevertheless improves the impedance estimates (see Figures 17-18).

SYNTHETICS EXAMPLES

Several models were used to test the inversion program. We present the inversion results of two sample models here. The first examined model is shown in Figure 10a. Both PP and PS synthetics have the same initial zero-phase (100 HZ Ricker) wavelet and the same offset range from 0 to 1000 m (Figure 10b and 10c). Because the 100 HZ ricker wavelet has less low-frequency components, the impedance estimation has significantly improved by BLIMP, Figures 13-14. Also the scale factor in BLIMP solves the $\Delta I/I$ and $\Delta J/J$ scaling problem to high percents, Figures 11-12.

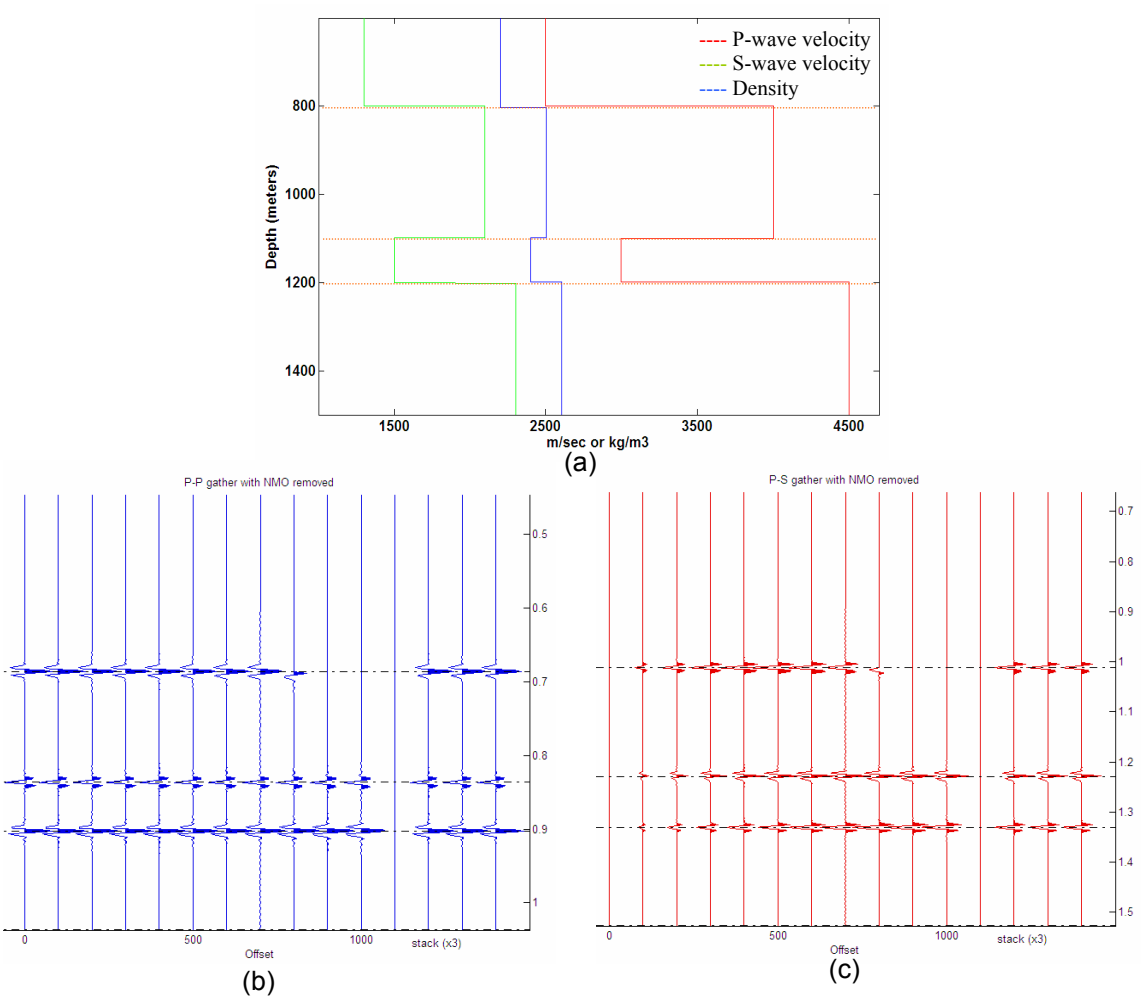

FIG. 10. (a) A simple log model in depth. (b) A synthetic CMP gather from the model in Figure 10a, in PP time. (c) A synthetic CCP gather from the model in Figure 10a, in PS time. In each seismogram, the three traces on the right are three repetitions of the stacked trace. Both seismograms have the initial 100 HZ zero-phase wavelet.

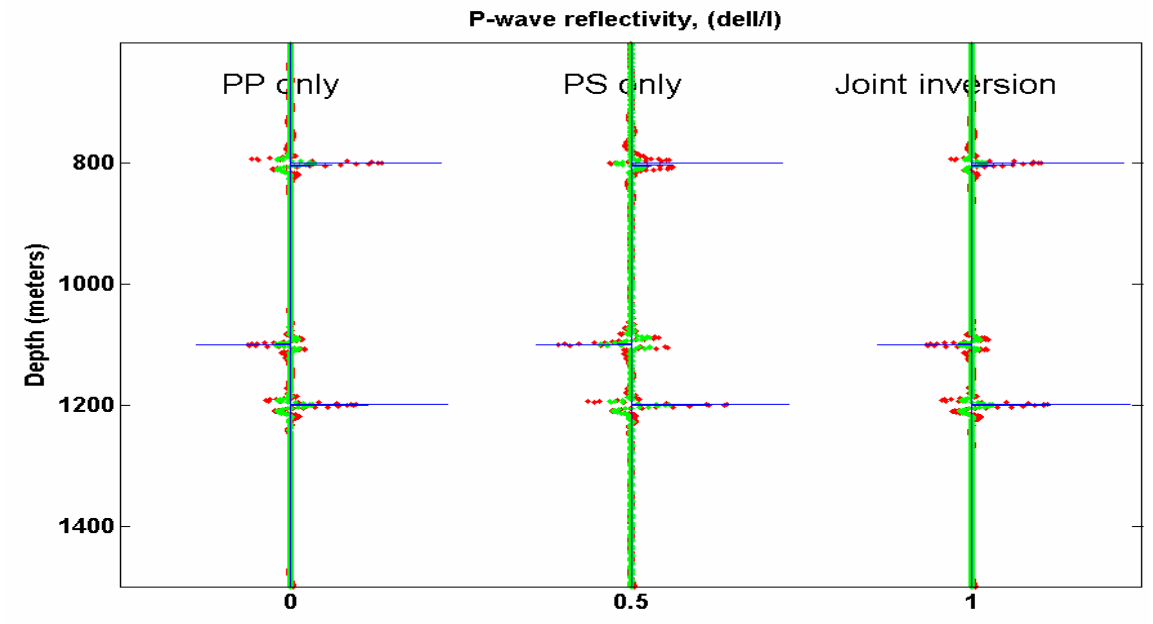

FIG. 11. (ΔI/I) as estimated from PP inversion only (left), PS inversion only (middle) and joint inversion (right), for the log model in Figure 10a. In each plot the red curve is ΔI/I calculated by code after restoring low-frequency content, the green curve is ΔI/I calculated by code before restoring low-frequency content and the blue curve is the real ΔI/I calculated directly from the model log of Figure 10a.

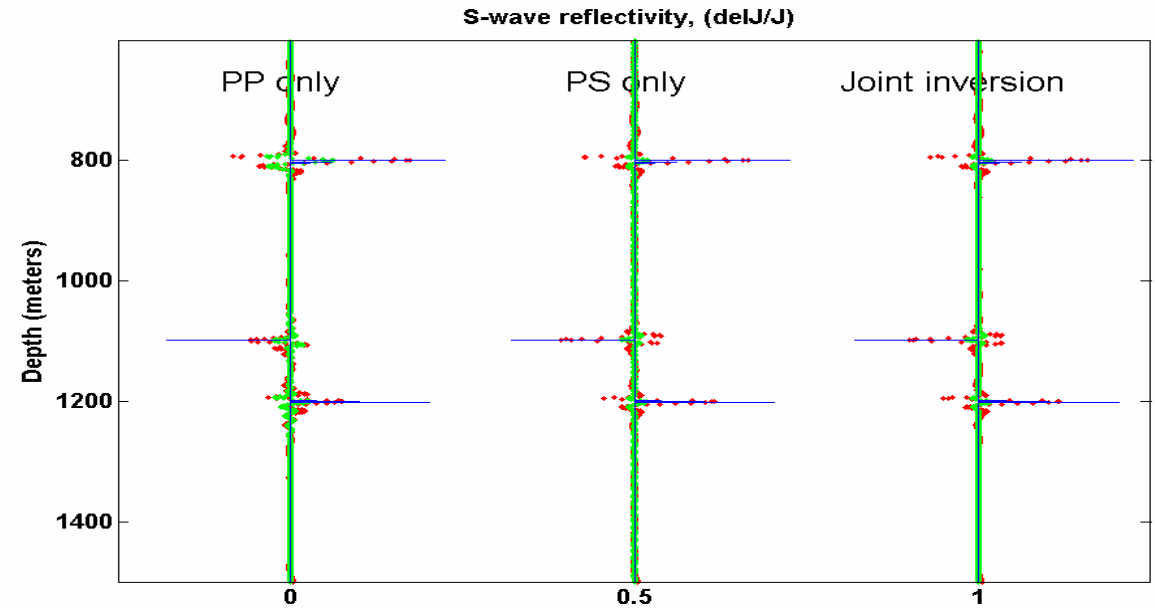

FIG 12. (ΔJ/J) as estimated from PP inversion only (left), PS inversion only (middle) and joint inversion (right), for the log model in Figure 10a. In each plot the red curve is ΔJ/J calculated by code after restoring low-frequency content, the green curve is ΔJ/J calculated by code before restoring low-frequency content, and the blue curve is the real ΔJ/J calculated directly from the model log of Figure 10a.

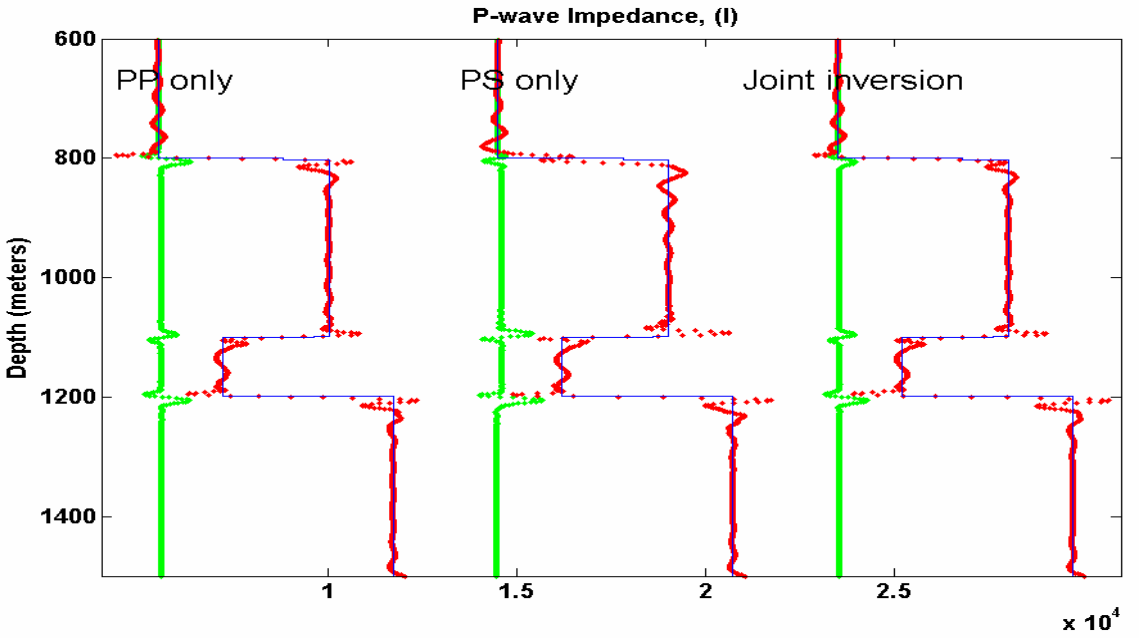

FIG. 13. P-wave Impedance (I) as estimated from PP inversion only (left), PS inversion only (middle) and joint inversion (right), for the log model in Figure 10a. In each plot, the red curve is estimated Impedance after restoring low-frequency content, green curve is estimated impedance before restoring low-frequency content, and the blue curve is the true impedance.

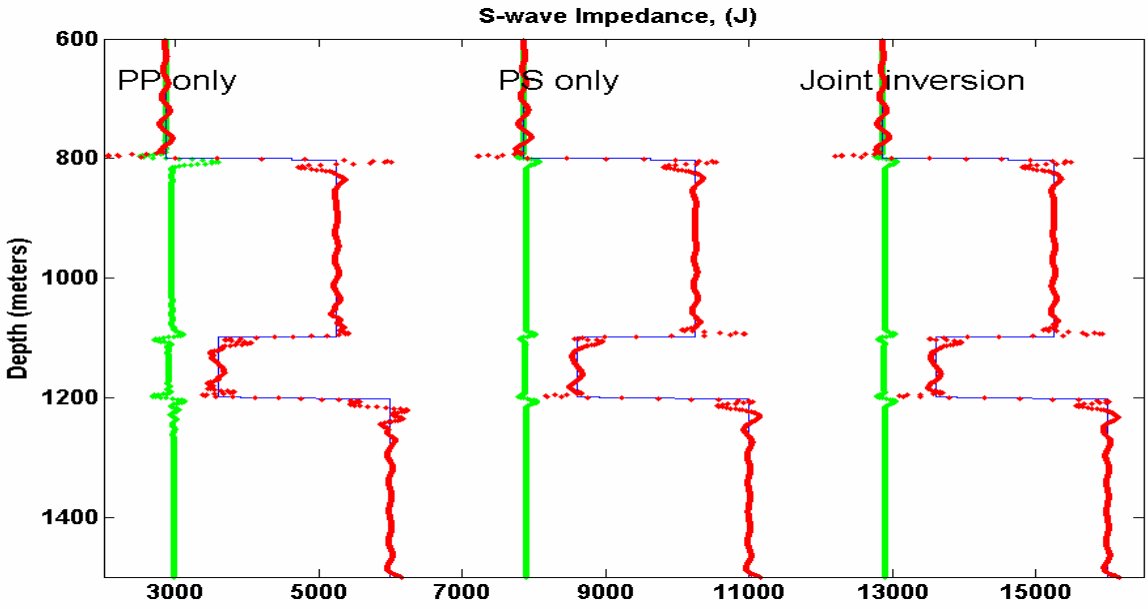

FIG. 14. S-wave Impedance (J) as estimated from PP inversion only (left), PS inversion only (middle) and joint inversion (right), for the log model in Figure 10a. In each plot the red curve is estimated Impedance after restoring low-frequency content, green curve is estimated impedance before restoring low-frequency content and the blue curve is the true impedance.

The second examined model is model in Figure 2a. This time the initial wavelet for generating the PP and PS synthetics, is a zero-phase 10-80 HZ (Butterworth) wavelet, which has a band-width of 5-10-80-100 (Figures 2b and 2c). Using this wavelet, the synthetics have ample low-frequency content. However the low-frequency restoration has improved the impedance estimation, Figures 17-18. In these Figures the red plots, the inversion results after low-frequency restoration, shows P- and S-wave impedances has reasonable results and very near to true values (blue plots).

Figures 15 and 16 show the $\Delta I/I$ and $\Delta J/J$ of the simple logs model (Figure 2a) by PP inversion only, PS inversion only and joint inversion, respectively. As it shown in Figure 15, the scaling problem of estimation $\Delta I/I$ is nicely treated after restoring the low-frequency content in red plots. Also Figure 16 shows that comparing to PP and PS inversion only, the joint inversion has better result for $\Delta J/J$ estimation.

The errors of $\Delta I/I$ and $\Delta J/J$ estimation, for all three inversion methods is due to the increase in error of the Zoeppritz equation approximations with increasing offset (Larsen, 1999). Also the deviation in relationship between density and compressional impedance (in our previous assumption, $\frac{\Delta\rho}{\rho} = \frac{1}{5}\frac{\Delta I}{I}$), caused some error in the inversion results.

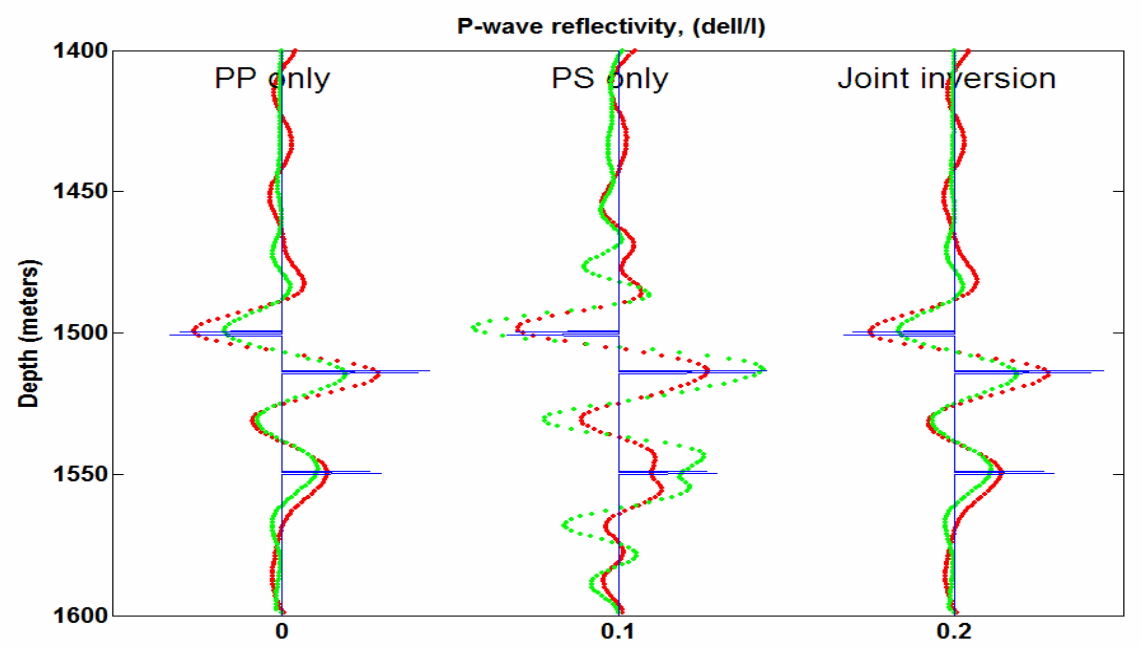

FIG. 15. (ΔI/I) as estimated from PP inversion only (left), PS inversion only (middle) and joint inversion (right), for the log model in Figure 2a. In each plot, the red curve is ΔI/I calculated by code after restoring low-frequency content, the green curve is ΔI/I calculated by code before restoring low-frequency content, and the blue curve is the real ΔI/I calculated directly from the model log of Figure 2a.

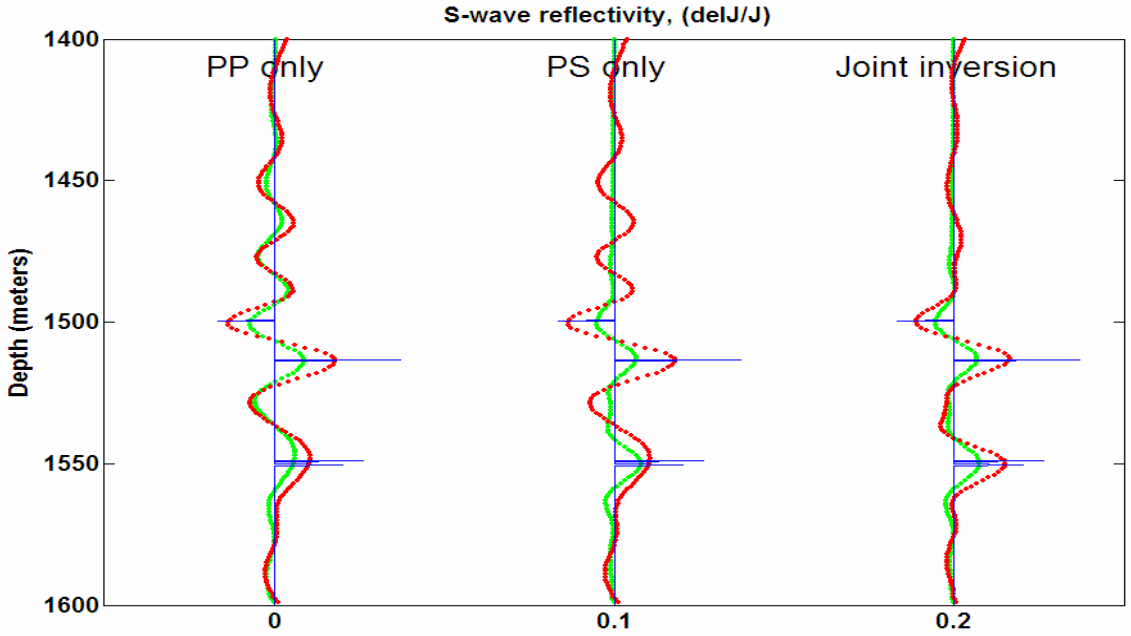

FIG. 16. (ΔJ/J) as estimated from PP inversion only (left), PS inversion only (middle), and joint inversion (right), for the log model in Figure 2a. In each plot the red curve is ΔJ/J calculated by code after restoring low-frequency content, the green curve is ΔJ/J calculated by code before restoring low-frequency content, and the blue curve is the real ΔJ/J calculated directly from the model log of Figure 2a.

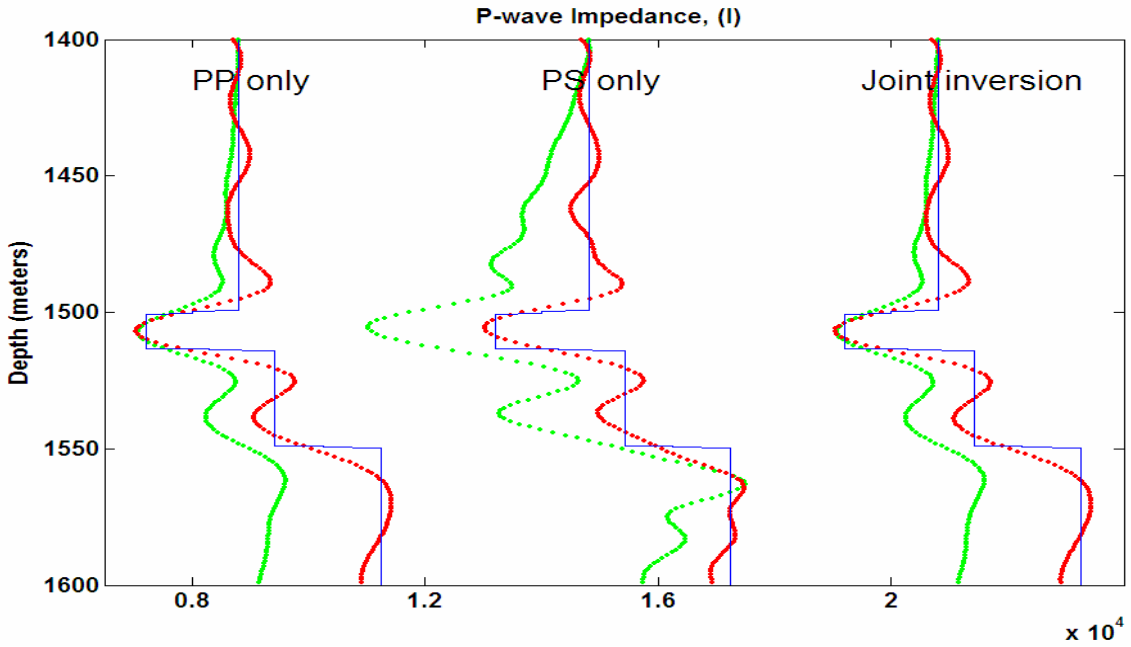

FIG. 17. P-wave Impedance (I) as estimated from PP inversion only (left), PS inversion only (middle) and joint inversion (right), for the log model in Figure 2a. In each plot the red curve is estimated Impedance after restoring low-frequency content, the green curve is estimated impedance before restoring low-frequency content, and the blue curve is the true impedance.

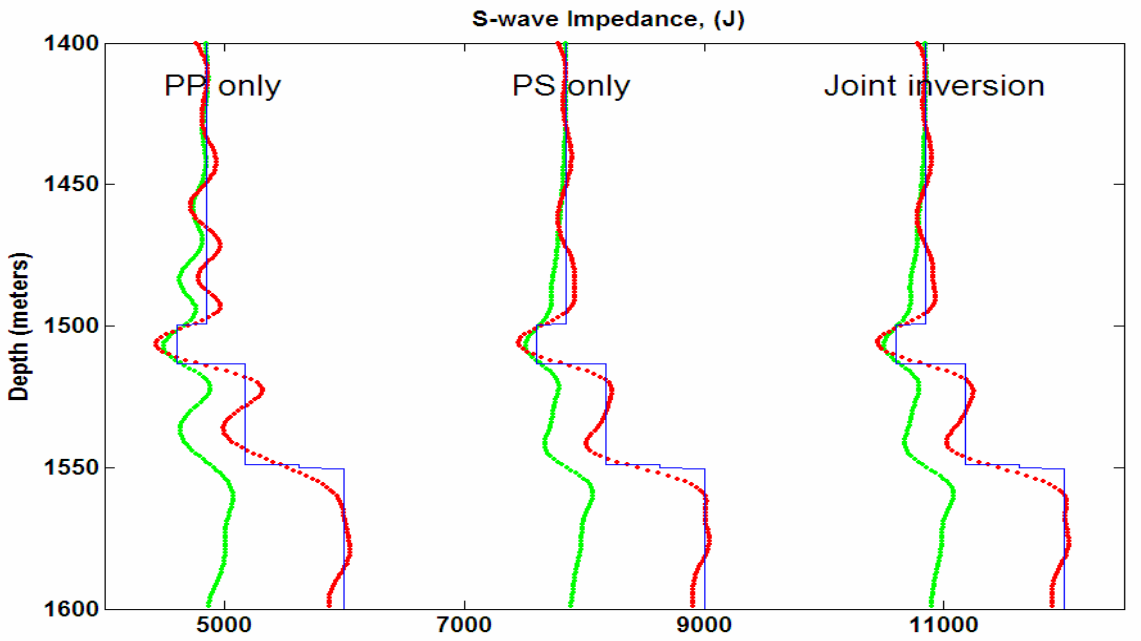

FIG. 18. S-wave Impedance (J) as estimated from PP inversion only (left), PS inversion only (middle) and joint inversion (right), for the log model in Figure 2a. In each plot the red curve is estimated Impedance after restoring low-frequency content, the green curve is estimated impedance before restoring low-frequency content, and the blue curve is the true impedance.

Although for the elastic media, based on Zoeppritz equations, reflection coefficients are all real and independent of frequency (pre-critical angle), the resolution is frequency dependent. Consequently, adding low-frequency trend will result into improving the resolution of inversion results, Figures 17 and 18.

A summary of the inversion procedure including low-frequency compensation is shown in Figure 19. In the following section, the inversion program result for a real log is examined.

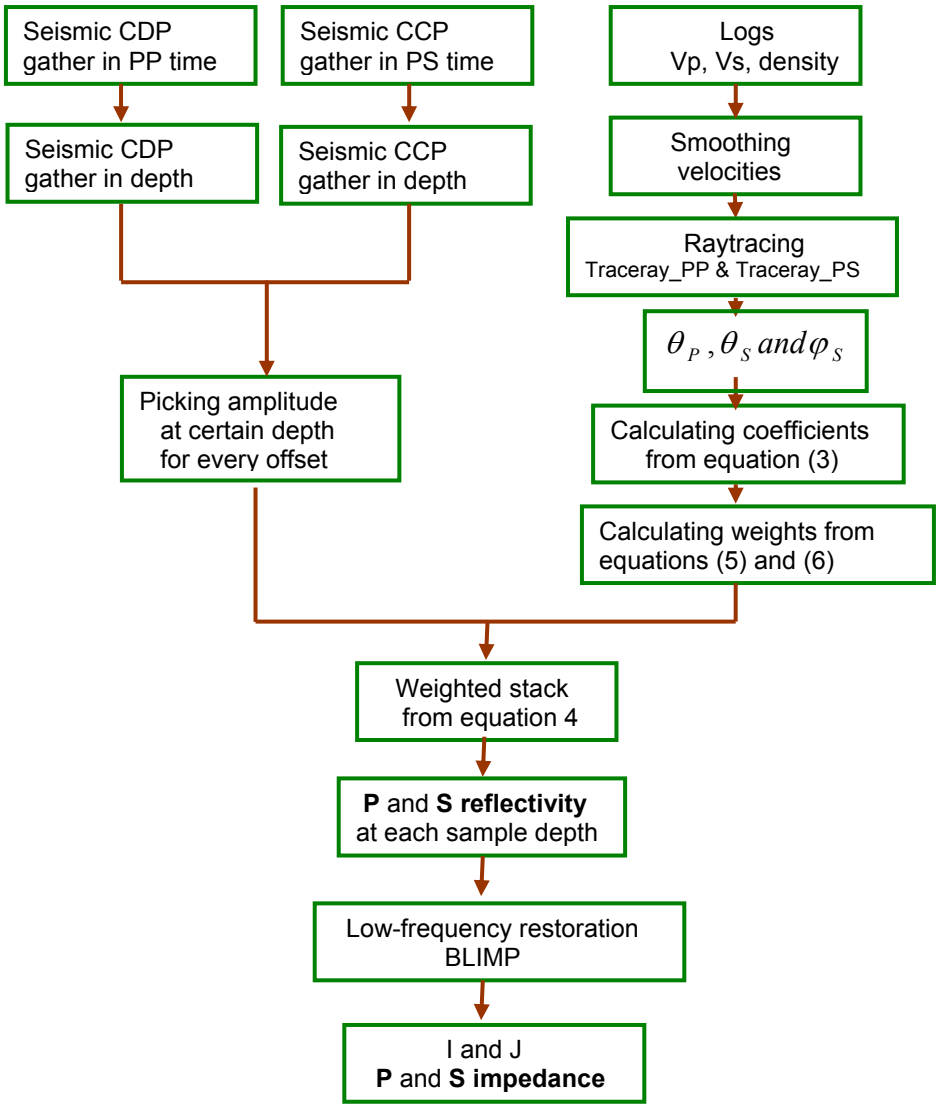

FIG. 19. A schematic algorithm explaining the procedure of the joint inversion.

REAL LOG EXAMPLE

The inversion results for the real log model of Figure 20a, is examined. The example comes from Blackfoot Field, owned and operated by Encana, in southeastern Alberta, Canada. In these Figures the Butterworth wavelet is used for both PP and PS synthetics and the same offset range from 0 to 1000 m. The stacking weights required to estimate $\Delta I/I$ and $\Delta J/J$ for the logs model in Figure 20a, are shown in Figures 21 and 22, respectively.

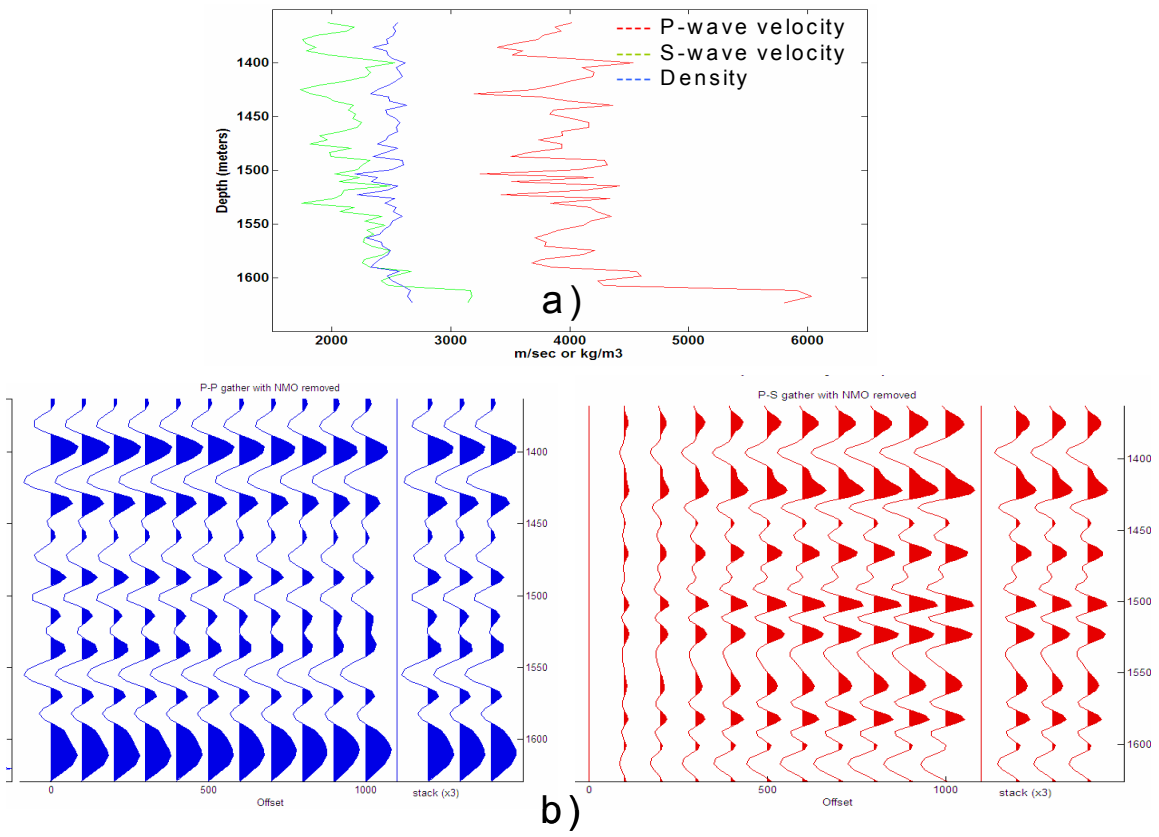

FIG. 20. (a) Real well logs at Blackfoot Field. (b) The PP and PS synthetics in depth. The three traces on the right are three repetitions of the stacked trace. Both seismograms have the initial butterworth wavelet.

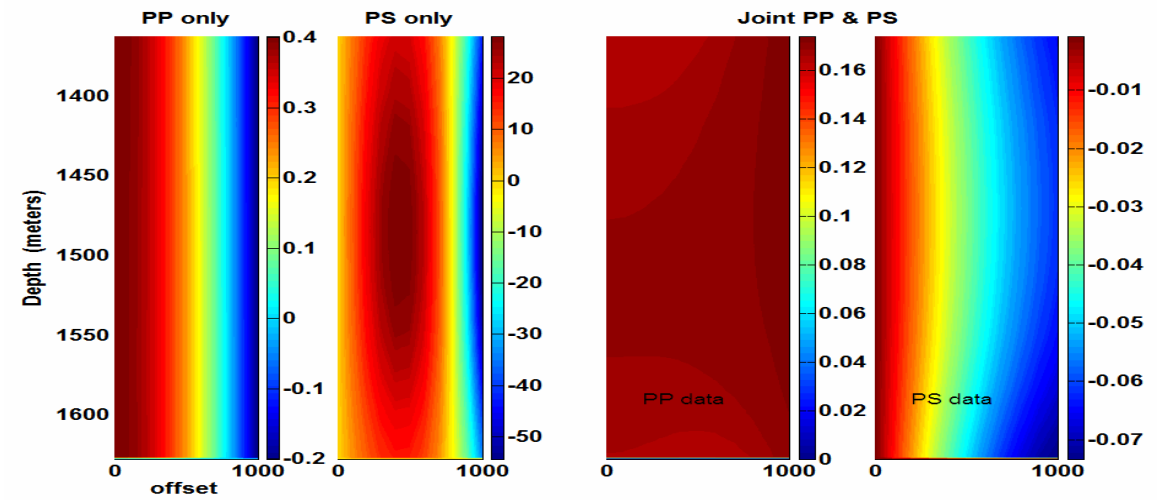

FIG. 21. The stacking weights required to estimate ΔI/I in PP method (left) and PS method (middle) and joint PP and PS method (right), for the logs model in Figure 20a. The joint method needs two sets of weights, for PP and PS data. Note the colour bars on the right of each plot.

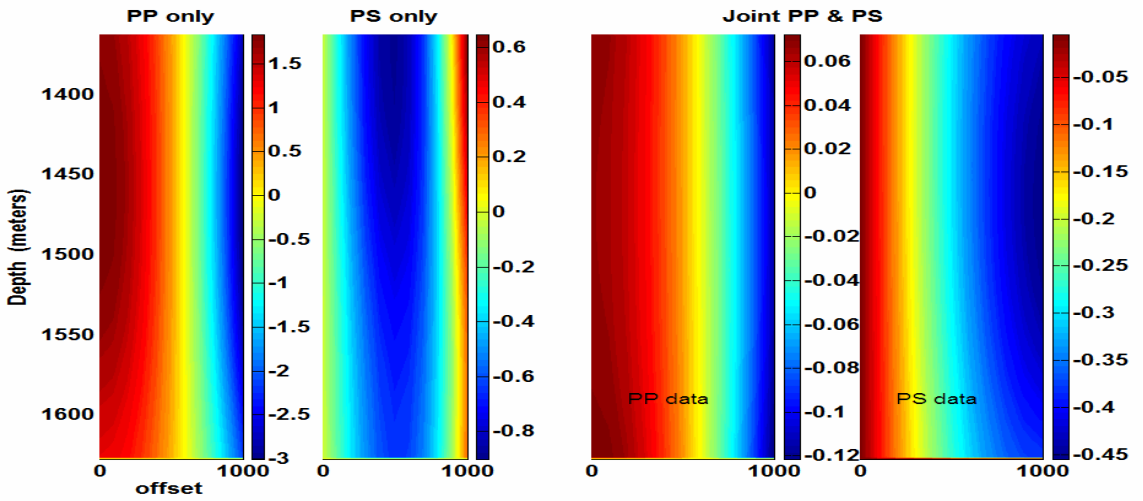

FIG. 22. The stacking weights required to estimate ΔJ/J in PP method (left) and PS method (middle) and joint PP and PS method (right), for the logs model in Figure 20a. The joint method needs two sets of weights, for PP and PS data. Note the colour bars on the right of each plot.

In Figures 23–28, the inversion results for the real log model of Figure 20a, is examined. In these Figures the trace of estimated $\Delta I/I$ or $\Delta J/J$, calculated from model in Figure 20a, is repeated and compared to true $\Delta I/I$ or true $\Delta J/J$ (shown in the middle of each Figures). In all these Figures, correlation between estimated and true reflectivity is clear.

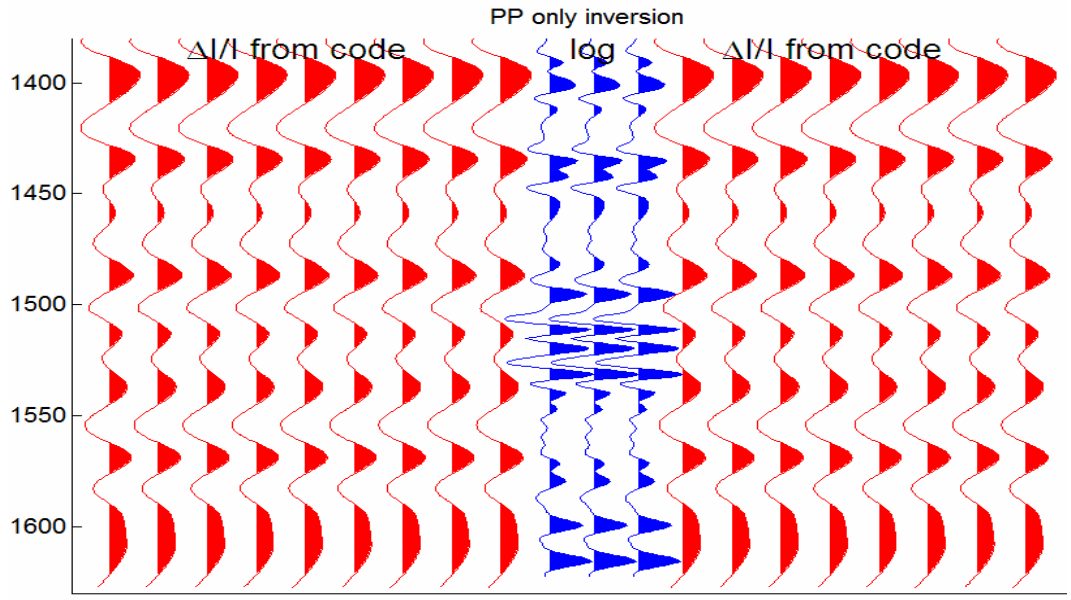

FIG. 23. The estimation of ΔI/I by PP inversion only, comparing to true ΔI/I from log in the middle. The blue traces are true ΔI/I from log and the red traces are estimated ΔI/I from code.

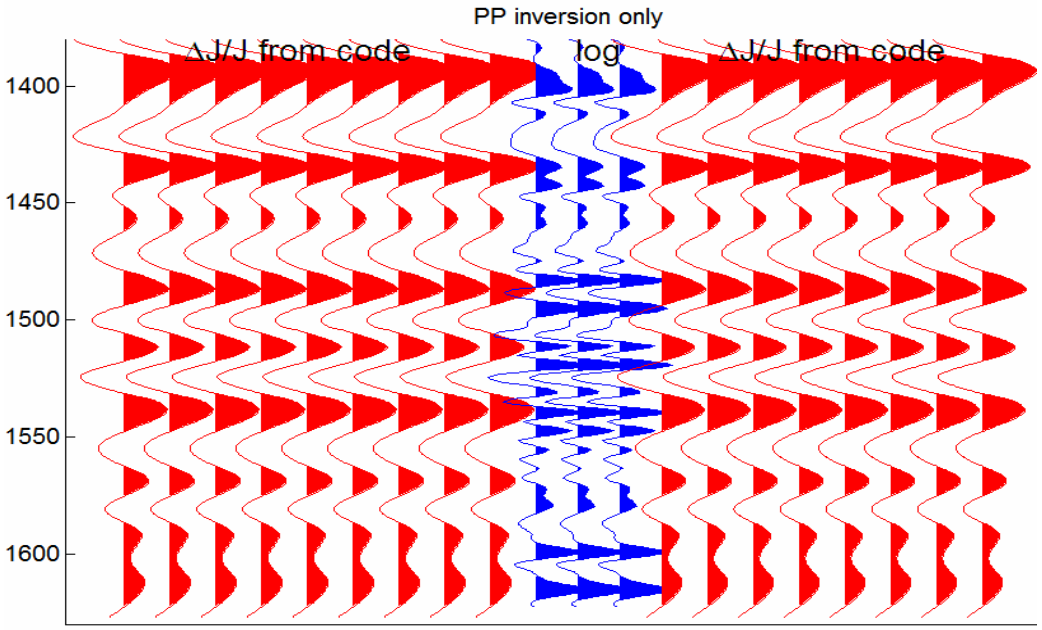

FIG. 24. The estimation of ΔJ/J by PP inversion only, comparing to true ΔJ/J from log in the middle. The blue traces are true ΔJ/J from log and the red traces are estimated ΔJ/J from code.

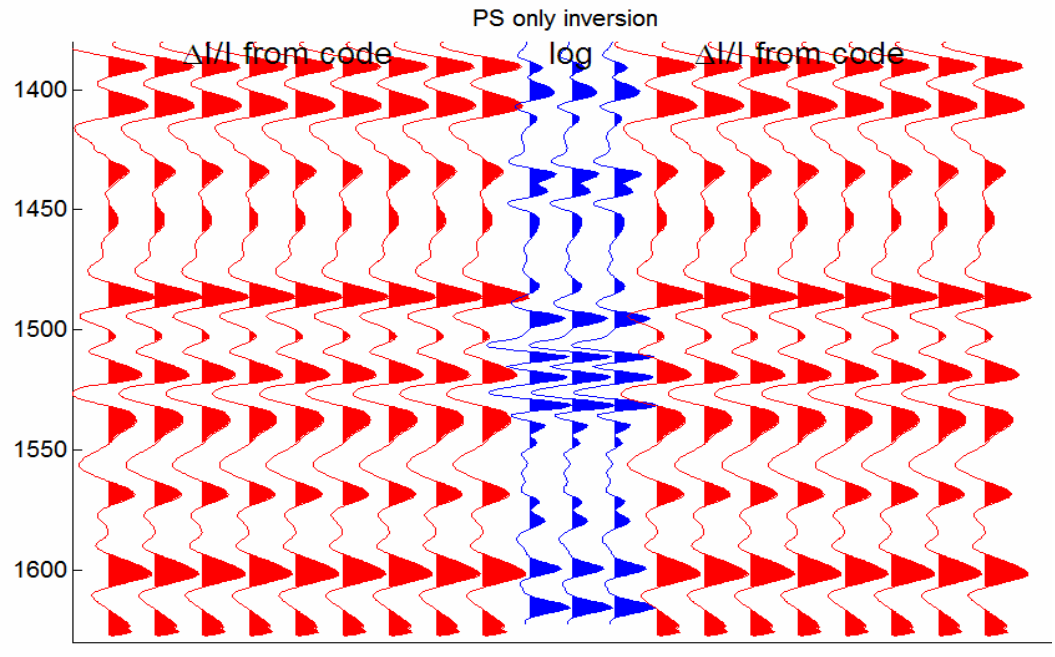

FIG. 25. The estimation of ΔI/I by PS inversion only, comparing to true ΔI/I from log in the middle. The blue traces are true ΔI/I from log and the red traces are estimated ΔI/I.

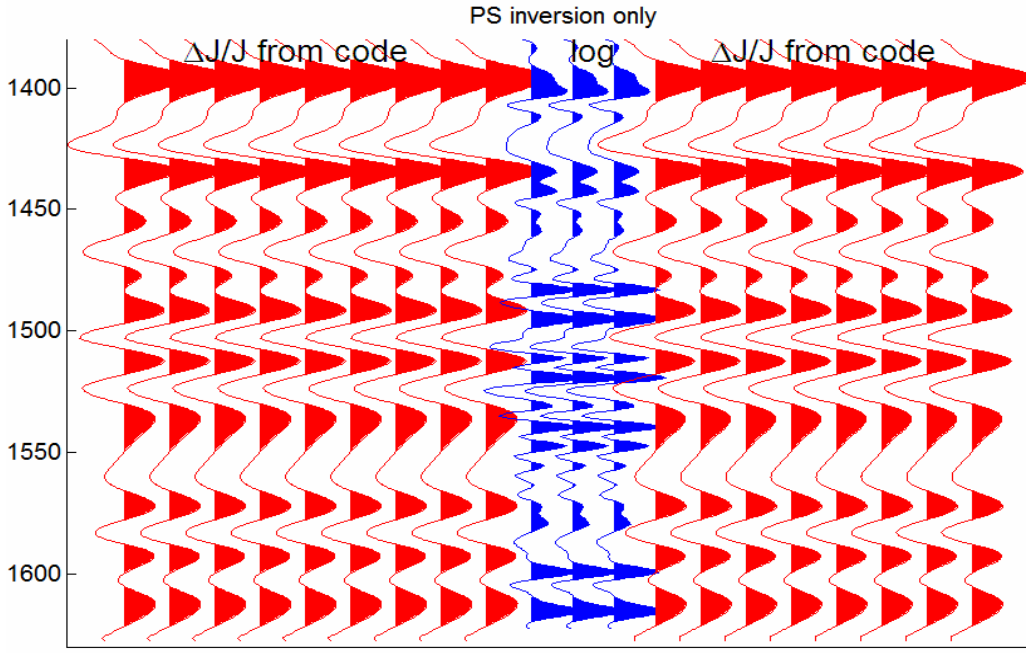

FIG. 26. The estimation of ΔJ/J by PS inversion only, comparing to true ΔJ/J from log in the middle. The blue traces are true ΔJ/J from log and the red traces are estimated ΔJ/J.

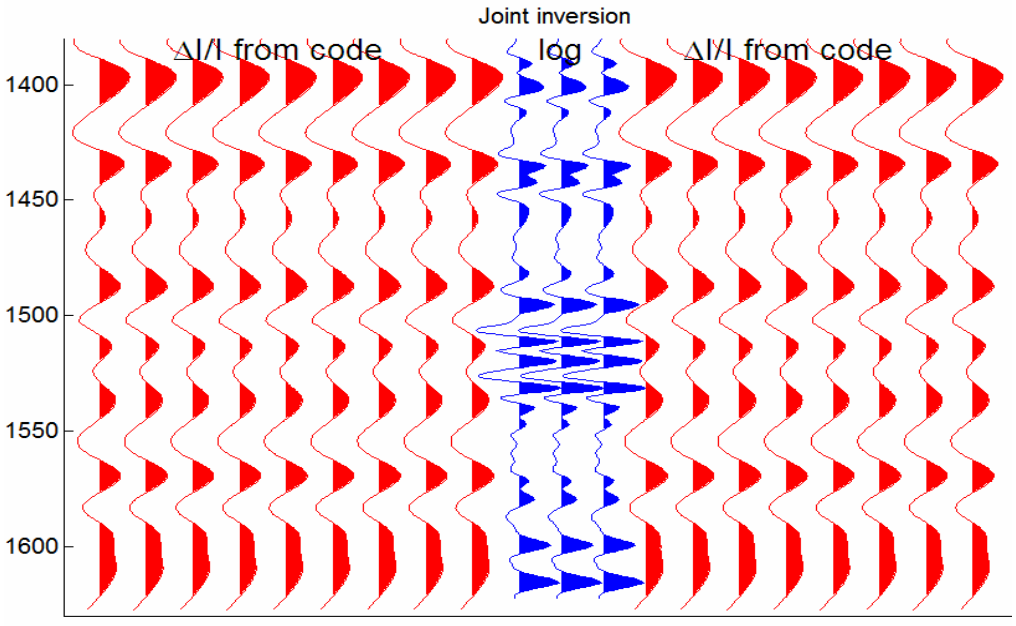

FIG. 27. The estimation of ΔI/I by joint inversion only, comparing to true ΔI/I from log in the middle. The blue traces are true ΔI/I from log and the red traces are estimated ΔI/I.

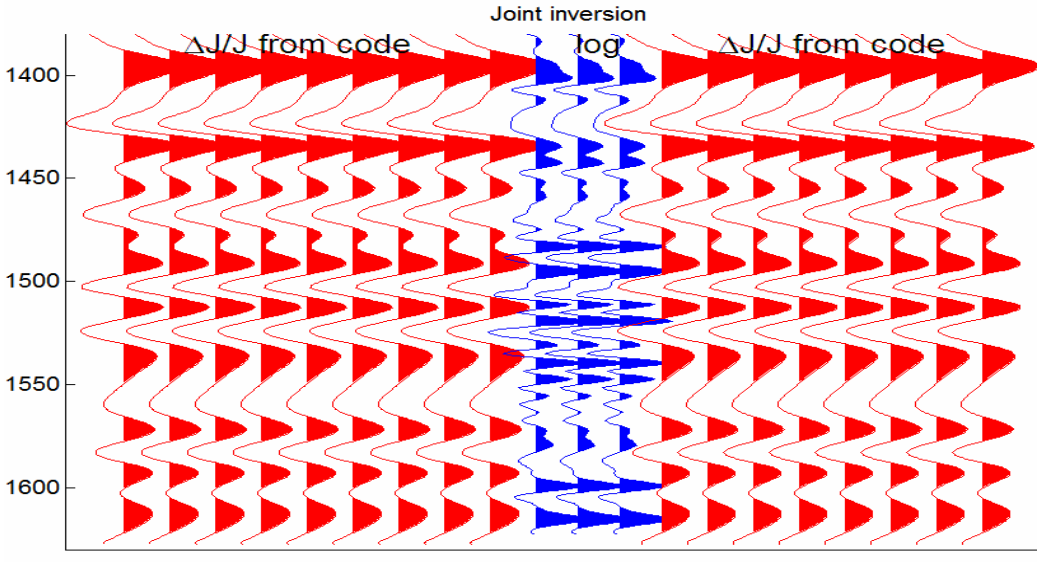

FIG. 28. The estimation of ΔJ/J by Joint inversion only, comparing to true ΔJ/J from log in the middle. The blue traces are true ΔJ/J from log and the red traces are estimated ΔJ/J.

For real log model, Figure 20a, the impedance estimation by all three methods is examined. Impedance estimation has significantly improved by low-frequency restoration, Figures 29-31. In these Figures a very good match between true impedances and estimated impedances is clear.

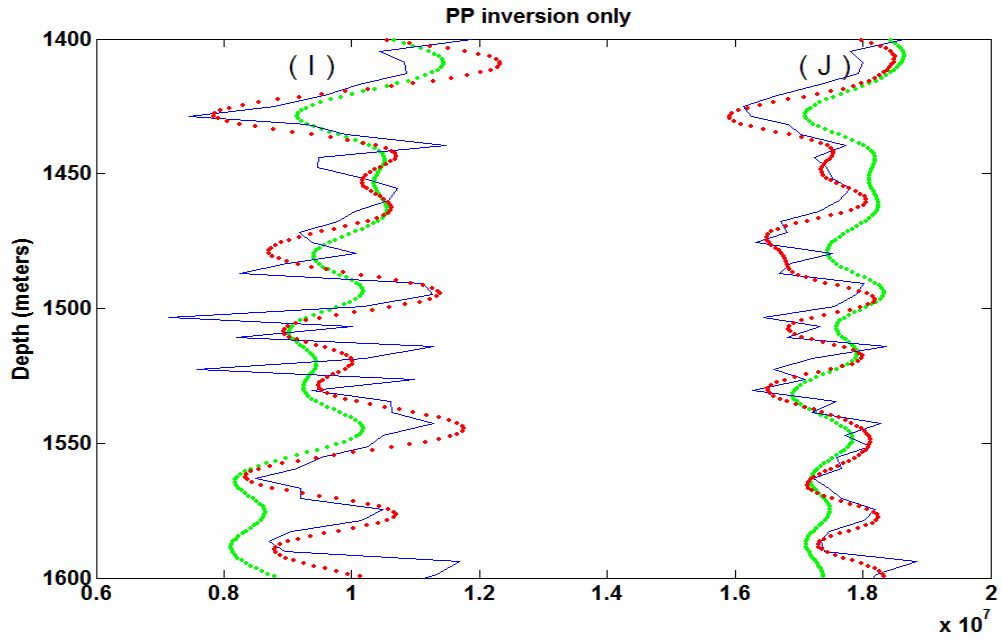

FIG. 29. P-wave Impedance (I) and S-wave impedance (J) as estimated from PP inversion only, for the model in Figure 10a. In each plot the red curve is estimated Impedance after restoring low-frequency content, the green curve is estimated impedance without restoring low-frequency content, and the blue curve is the true impedance.

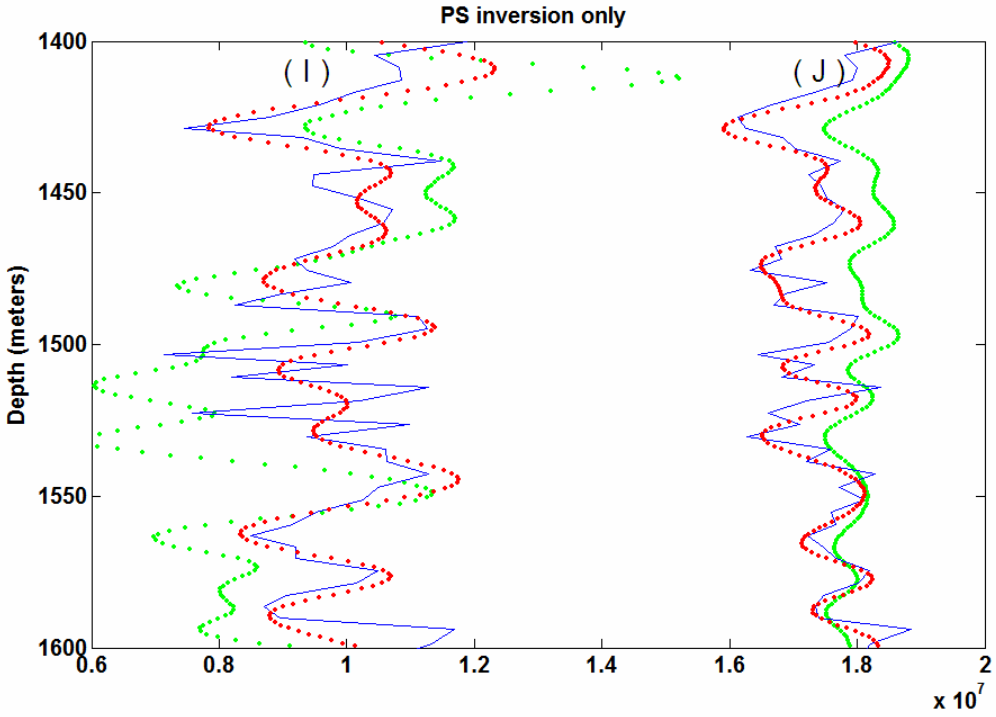

FIG. 30. P-wave Impedance (I) and S-wave impedance (J) as estimated from PS inversion only, for the model in Figure 10a. In each plot the red curve is estimated Impedance after restoring low-frequency content, the green curve is estimated impedance without restoring low-frequency content, and the blue curve is the true impedance.

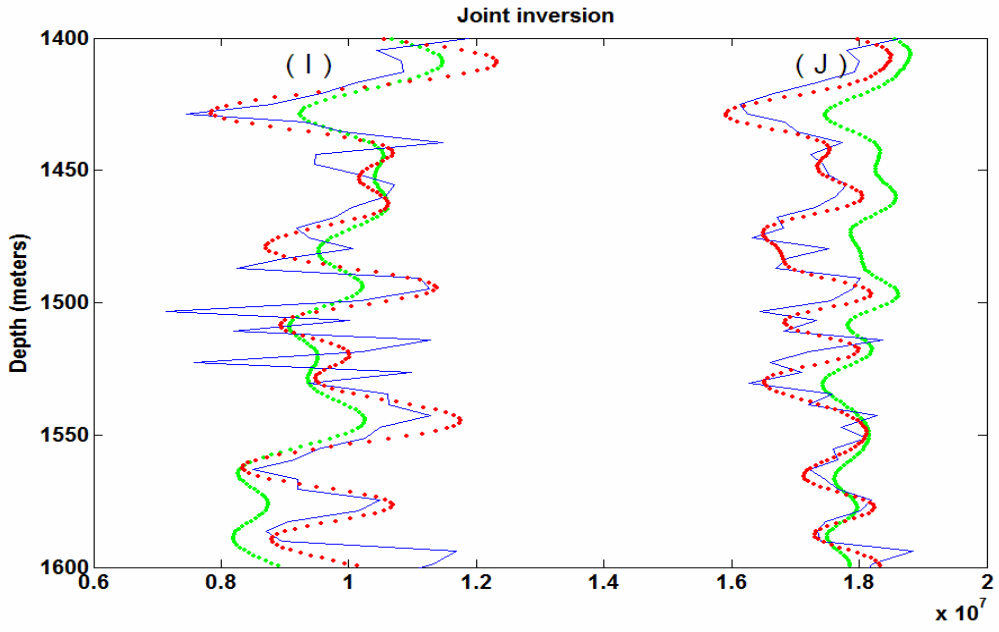

FIG. 31. P-wave Impedance (I) and S-wave impedance (J) as estimated from Joint inversion only, for the model in Figure 10a. In each plot the red curve is estimated Impedance after restoring low-frequency content, the green curve is estimated impedance without restoring low-frequency content, and the blue curve is the true impedance.

In real seismic sections, the PP and PS data have different frequency content. Typically PS data have less frequency content comparing to PP data. To simulate this PP and PS synthetics were generated with different input wavelets. To generate synthetics sections with different frequency content, the zero-phase wavelet 5-10-80-100 (butterworth wavelet) is used for PP synthetics and zero-phase wavelet 5-10-30-40 is used for PS synthetics (Figure 32).

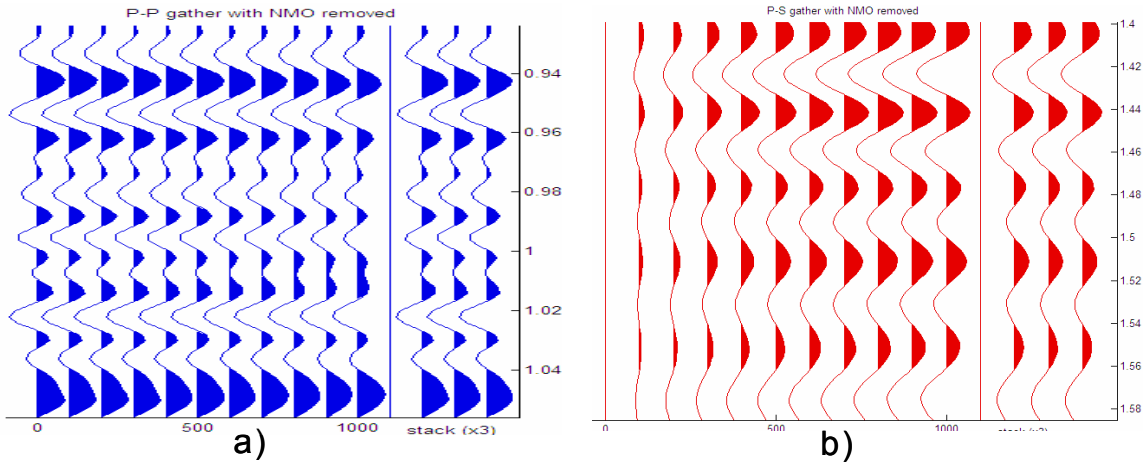

FIG. 32. A synthetic CMP gather from the model in Figure 20a, in PP time. (c) A synthetic CCP gather from the model in Figure 19a, in PS time. In each seismogram, the three traces on the right are three repetitions of the stacked trace.

In Figures 33 and 34 the repetition of estimated $\Delta I/I$ and $\Delta J/J$ from data shown in Figure 32 and 20b, is compared to true $\Delta I/I$ and $\Delta J/J$ (from the log model in Figure 20a). In all these Figures, correlation between estimated and true reflectivity is clear.

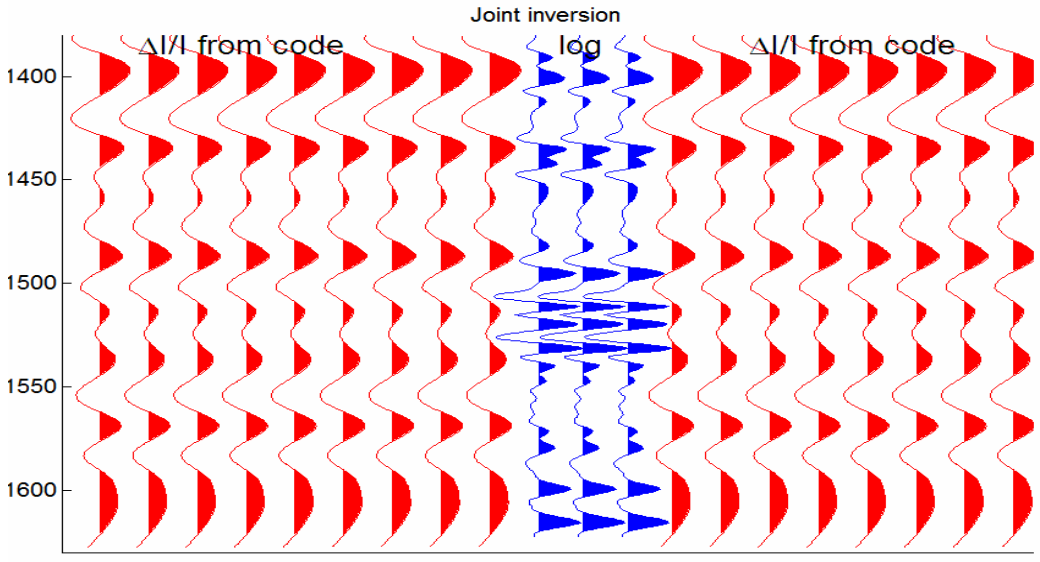

FIG. 33. The estimation of ΔI/I by joint inversion only, compared to true ΔI/I from log in the centre. The blue traces show true ΔI/I from log and the red traces are estimated ΔI/I.

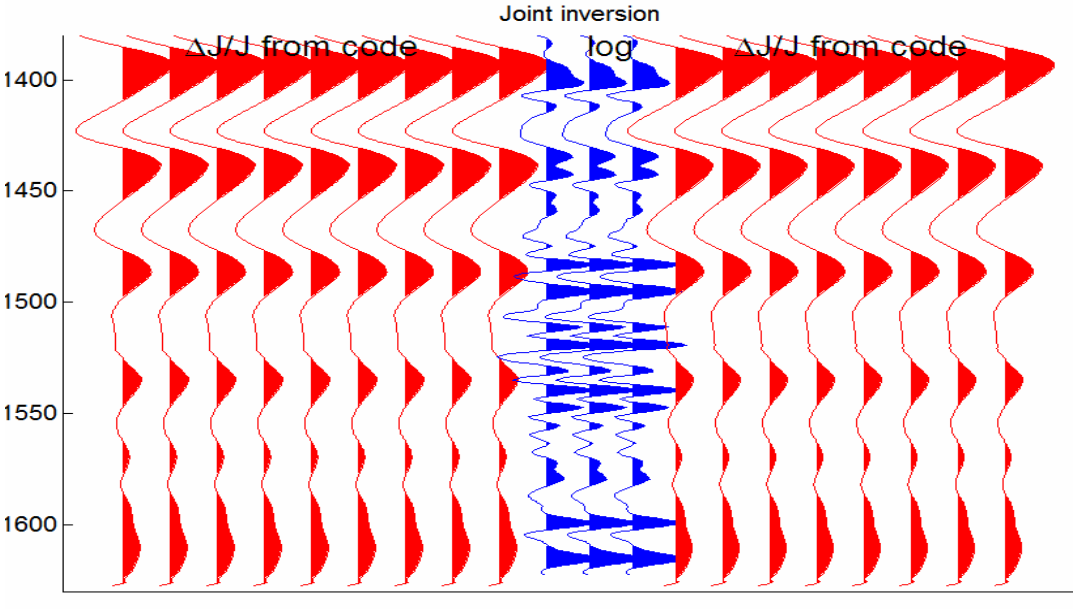

FIG. 34. The estimation of ΔJ/J by Joint inversion only, comparing to true ΔJ/J from log in the middle. The blue traces are true ΔJ/J from log and the red traces are inverted ΔJ/J.

For synthetics sections, Figure 32, the impedance estimation by joint inversion is examined. Impedance estimation has significantly improved by low-frequency restoration, Figures 35. In Figure 35, a very good match between true impedances and estimated impedances is clear.

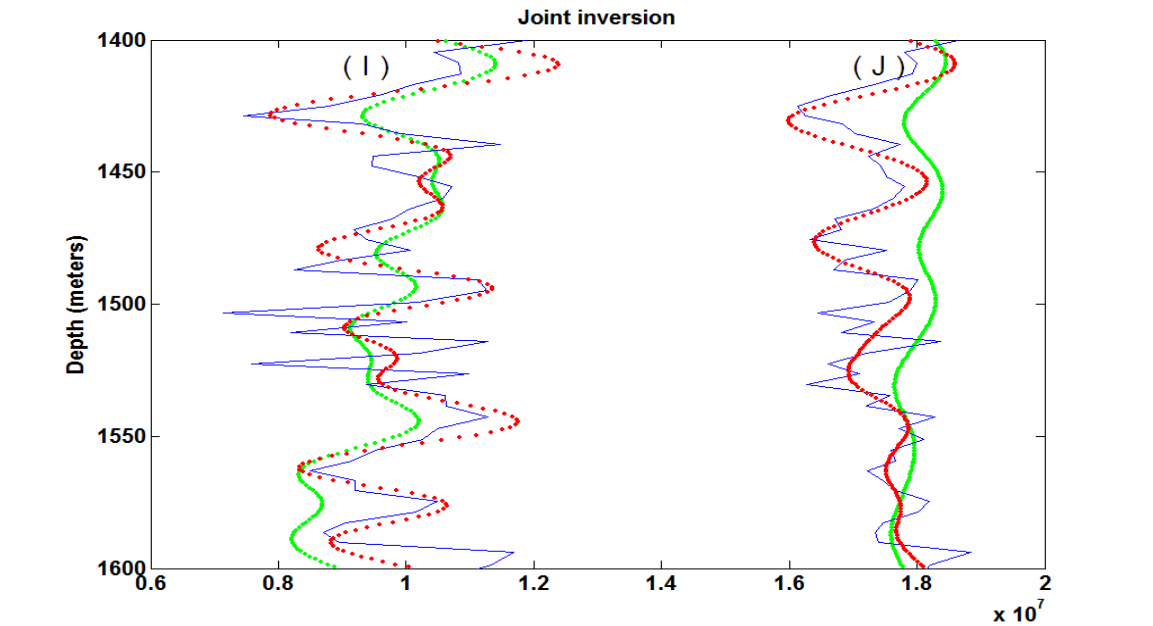

FIG. 35. P-wave Impedance (I) and S-wave impedance (J) as estimated from joint inversion for the data in Figure 32. In each plot the red curve is estimated Impedance after restoring low-frequency content, the green curve is estimated impedance without restoring low-frequency content, and the blue curve is the true impedance.

So far the inverted impedance reflectivity results from PP, PS-only inversion, and joint inversion are compared using synthetic noise-free data. To take a further step toward real data, all three methods are applied in the presence of noise. The inversion result with noisy data is presented in next section.

INVERSION RESULTS IN THE PRESENCE OF NOISE

Any given seismic recording will contain some amount of noise in relation to the desired signal. Among the most effective processing techniques, is the process of stacking over a range of offsets. Since a joint-inversion method includes twice as many reflectivity observations, it is reasonable to assume a corresponding improvement in signal-to-noise is possible (Larsen, 1999). In order to examine the effect of noise upon inversion accuracy, random noise was added to the synthetics data. Figure 36 shows the PP and PS synthetics of Figure 2b with the added noise. For this example, the noise is larger than is typically encountered in real surface seismic data.

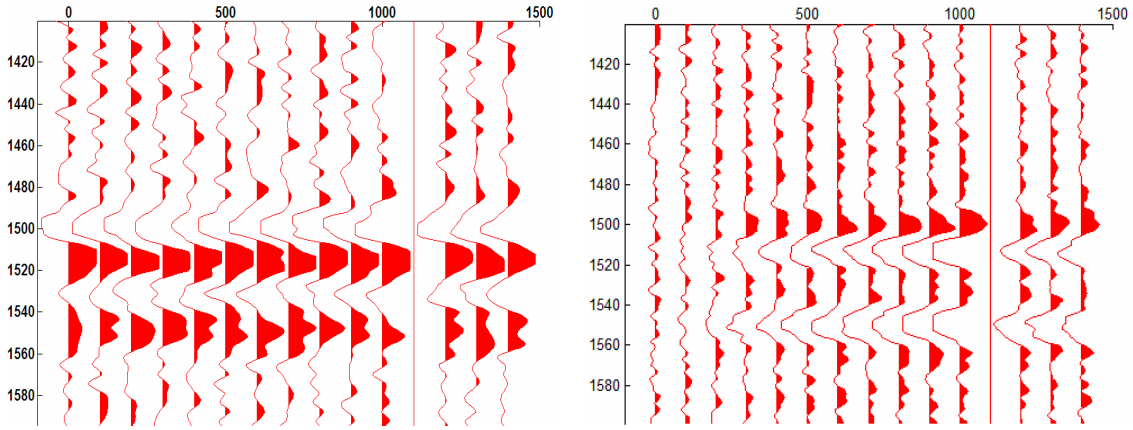

FIG. 36. (a) A synthetic CMP gather from the model in Figure 2a, in depth with signal-to-noise ratio of 2. (b) A synthetic CCP gather from the model in Figure 2a, in depth with signal-to-noise ratio of 2. In each seismogram, the three traces on the right are three repetitions of the stacked trace. Both seismograms have the initial Butterworth wavelet.

The $\Delta I/I$ and $\Delta J/J$ estimation of log model in Figure 2a, from noisy synthetics is shown in Figures 37 and 38, also the $\Delta I/I$ and $\Delta J/J$ estimation of log model in Figure 20a with the noisy synthetics data is shown in Figures 39-41. In all these Figures the red curve is estimated $\Delta I/I$ and $\Delta J/J$ from noise-free data, the green curve is estimated $\Delta I/I$ and $\Delta J/J$ from noisy data, and the blue curve is the true $\Delta I/I$ and $\Delta J/J$. As shown in Figure 37 and 40, in the presence of noise the PS inversion only is poor for $\Delta I/I$ estimation. Also, as shown in Figure 38 and 39, in the presence of noise the PP inversion only, is poor for $\Delta J/J$ estimation. Figures 37, 38, and 41 show very clearly that the joint inversion method has very good results for noisy data

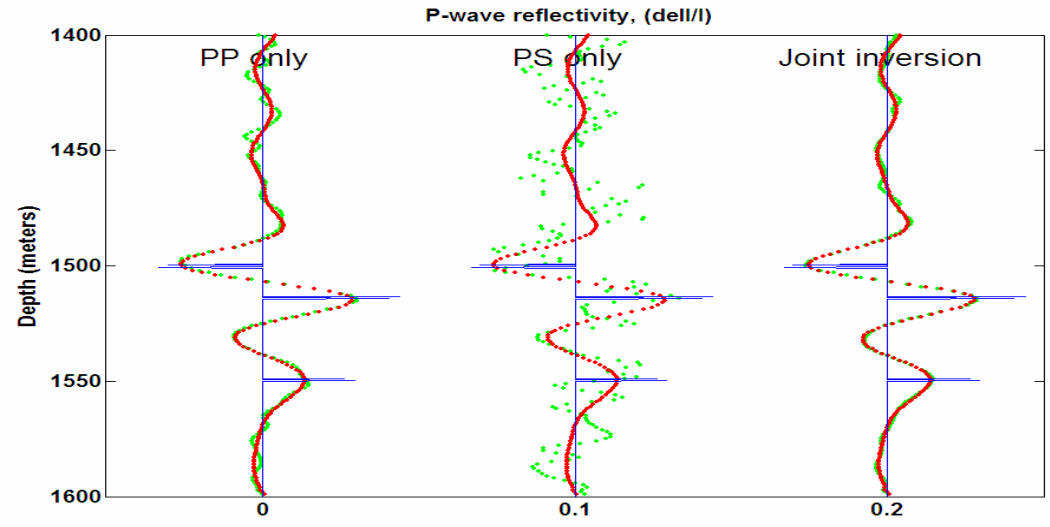

FIG. 37. (ΔI/I) as estimated from PP inversion only (left), PS inversion only (middle) and joint inversion (right), for the log model in Figure 2a with signal-to-noise ratio of 2. In each plot the red curve is estimated ΔI/I from noise-free data, the green curve is estimated ΔI/I from noisy data and the blue curve is the true ΔI/I.

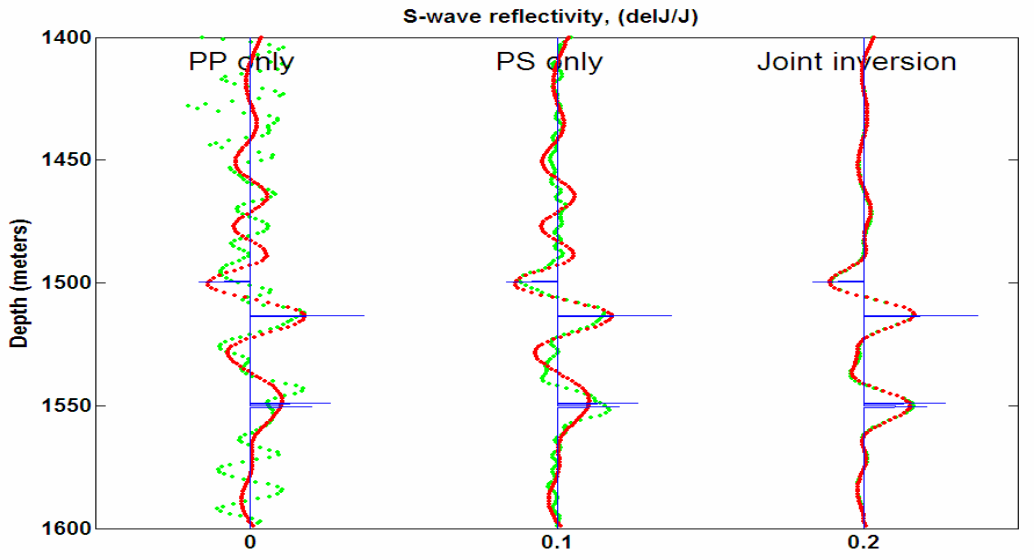

FIG. 38. (ΔJ/J) as estimated from PP inversion only (left), PS inversion only (middle) and joint inversion (right), for the log model in Figure 2a with signal-to-noise ratio of 2. In each plot the red curve is estimated ΔJ/J from noise-free data, the green curve is estimated ΔJ/J from noisy data, and the blue curve is the true ΔJ/J.

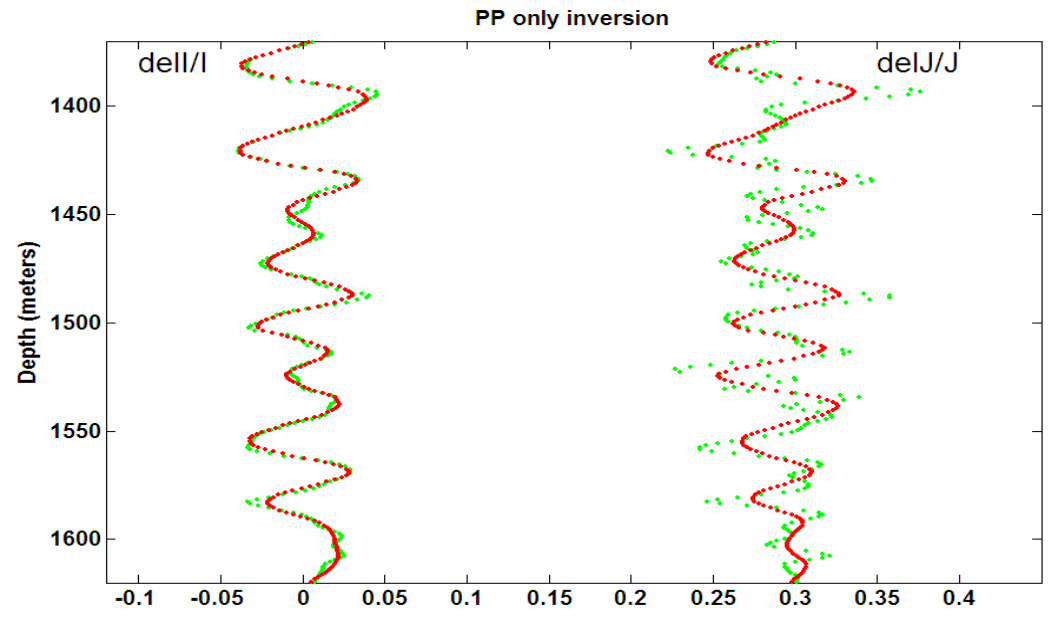

FIG. 39. (ΔI/I) and (ΔJ/J) as estimated from PP inversion only for the log model in Figure 20a with signal-to-noise ratio of 2. In each plot the red curve is estimated ΔI/I or ΔJ/J from noise-free data, green curve is estimated ΔI/I or ΔJ/J from noisy data, and the blue curve is the true ΔI/I or ΔJ/J.

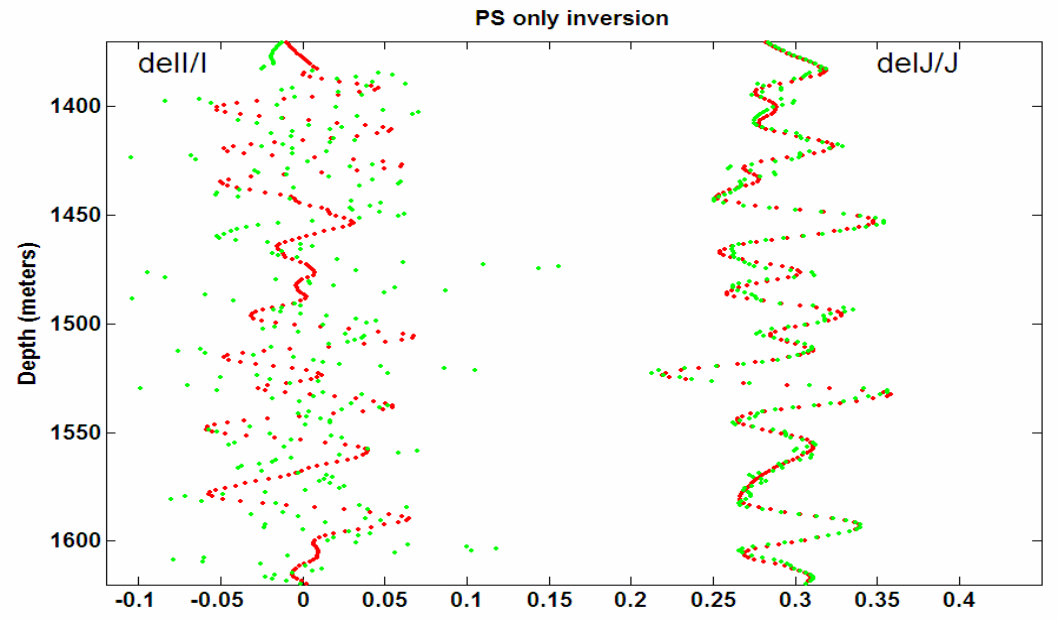

FIG. 40. (ΔI/I) and (ΔJ/J) as estimated from PS inversion only for the log model in Figure 20a with signal-to-noise ratio of 2. In each plot the red curve is estimated ΔI/I or ΔJ/J from noise-free data, the green curve is estimated ΔI/I or ΔJ/J from noisy data and the blue curve is the true ΔI/I or ΔJ/J.

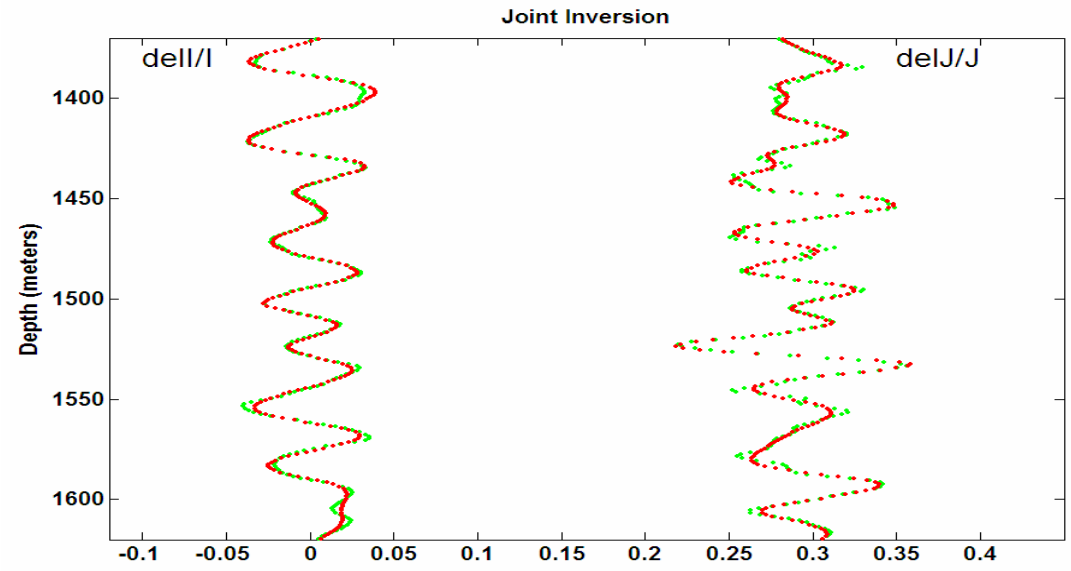

FIG. 41. (ΔI/I) and (ΔJ/J) as estimated from joint inversion the log model in Figure 20a with signal-noise ratio of 2. In each plot the red curve is estimated ΔI/I or ΔJ/J from noise-free data, green curve is estimated ΔI/I or ΔJ/J from noisy data and the blue curve is the true ΔI/I or ΔJ/J.

The I and J estimation of log model in Figure 20a, from noisy synthetics is shown in Figures 42 and 43. In all these Figures, the red curve is estimated $\Delta I/I$ and $\Delta J/J$ from noise-free data, the green curve is estimated $\Delta I/I$ and $\Delta J/J$ from noisy data and the blue curve is the true $\Delta I/I$ and $\Delta J/J$. As shown in Figure 43, in the presence of noise the PS inversion only is poor for $\Delta I/I$ estimation. Also as shown in Figure 42, in the presence of noise the PP inversion only, is poor for $\Delta J/J$ estimation. Figure 44, shows very clearly that the joint inversion method has very good impedance estimation for noisy data.

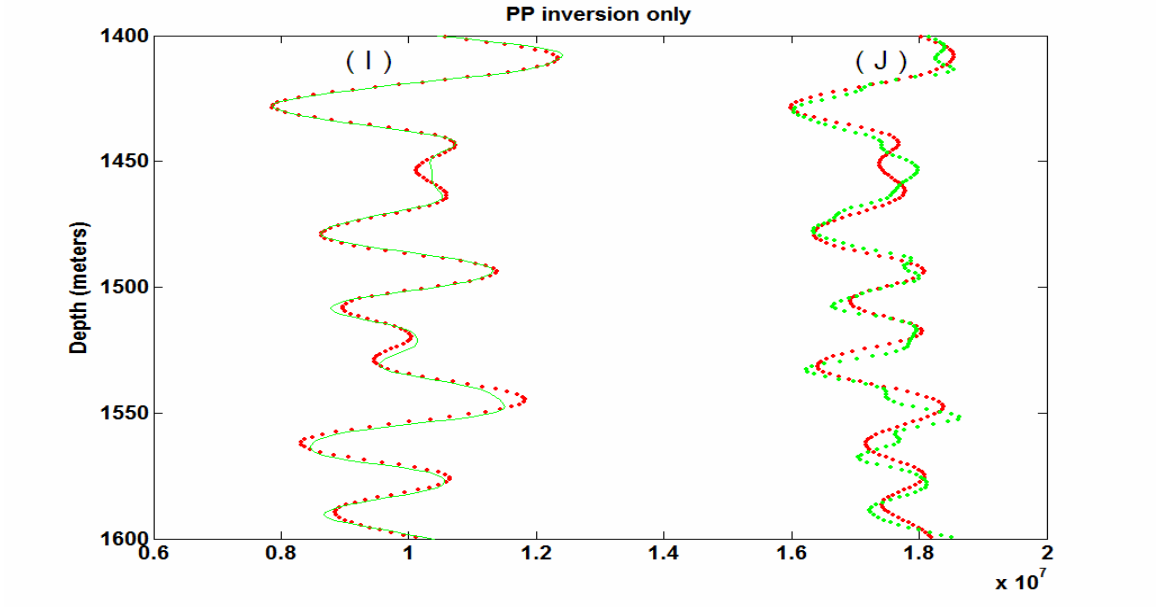

FIG. 42. I and J as estimated from PP inversion only for the log model in Figure 20a with signal-to-noise ratio of 2. In each plot, the red curve is impedance from noise-free data, the green curve is impedance estimated from noisy data, and the blue curve is the true impedance.

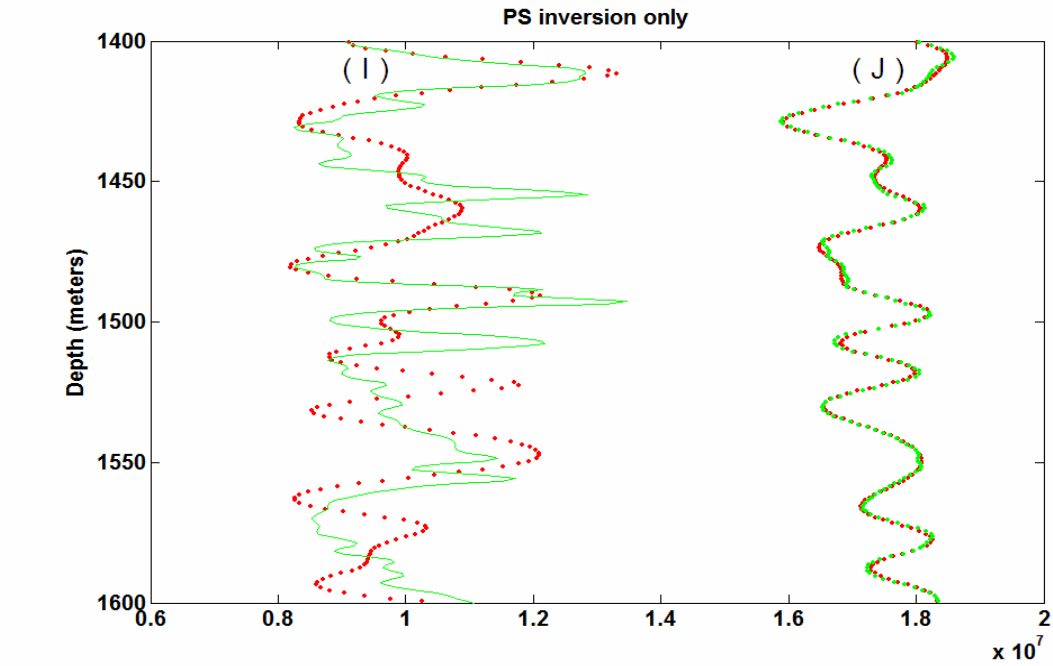

FIG. 43. I and J as estimated from PS inversion only for the log model in Figure 20a with signal-to-noise ratio of 2. In each plot, the red curve is impedance from noise-free data, the green curve is impedance estimated from noisy data, and the blue curve is the true impedance.

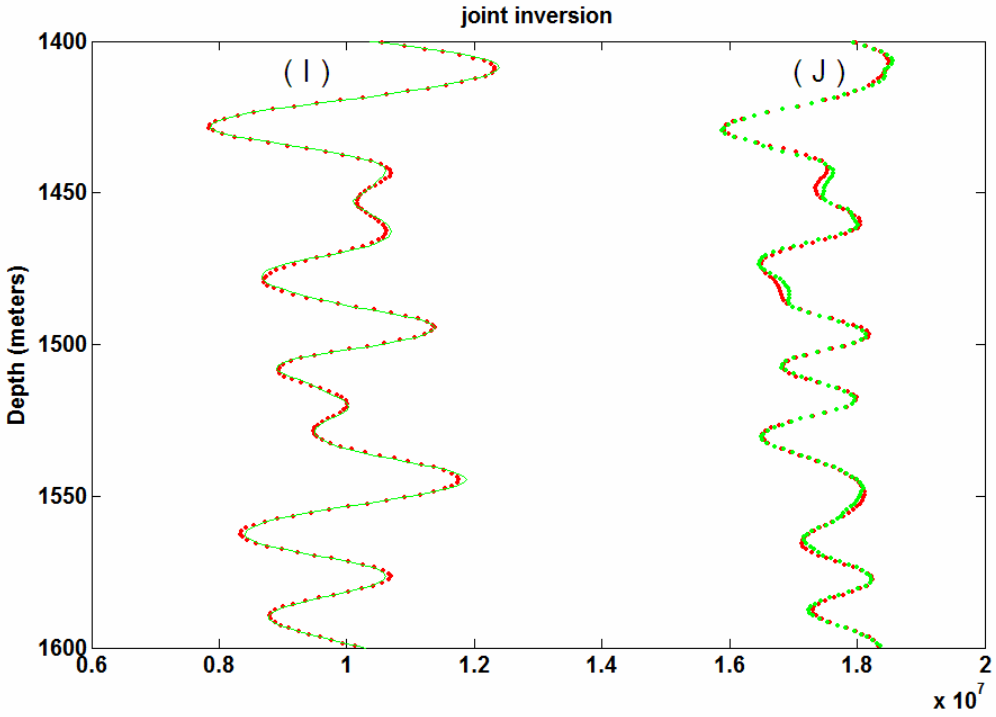

FIG. 44. I and J as estimated from joint inversion for the log model in Figure 20a with signal-to-noise ratio of 2. In each plot, the red curve is impedance from noise-free data, the green curve is impedance estimated from noisy data, and the blue curve is the true impedance.

CONCLUSIONS

The joint inversion program described by Larson (1999) has been cast as a MATLAB algorithm. This algorithm includes some modifications to Larsen's approach: (1) adding low-frequency trend to broadband data; (2) driving impedance estimation from P and S reflectivity. We showed that the adding the low-frequency trend can provide the impedance estimation significantly better that without restoration the low-frequency trend.

We documented the joint inversion performance in comparison with inversion with PP data only and with PS data only. It is shown that joint inversion was more accurate than PP and PS only inversion. We also showed that in presence of random noise, the joint inversion was significantly more accurate than other methods. This effect was the result of doubling the data fold input into estimation of P and S reflectivity.

ACKNOWLEDGEMENTS

We wish to thank to Mr. Kevin Hall for computer support and lots of help, and Ms. Brooke Berard and Mr. Jeff Thurston for proof-reading manuscripts and lots of discussion.

REFERENCES

Castagna, J.P., Batzle, M.L., and Eastwood , R.L., 1985, Relationships between compressional-wave and shear-wave velocities in clastic silicate rocks: Geophysics, **50**, 571-581.

Ferguson R.J., Margrave G.F., 1996, A simple algorithm for band-pass impedance inversion: CREWES Research Report, **8**, 1-10.

Larsen J.A., 1999, AVO inversion by simultaneous PP and PS inversion: M.Sc. Thesis, University of Calgary.

Lindseth R.O., 1979, Synthetic sonic logs – a process for stratigraphic interpretation: Geophysics, **44**, 3-26.

Margrave, G.F., Stewart R.R., and Larsen, J.A., 2001, Joint PP and PS seismic inversion: The Leading Edge, 1048-1052.

Smith, G.C. and Gidlow, P.M., 1987, Weighted stacking for rock property estimation and detection of gas: Geophysical Prospecting, **35**, 993-1014.

Stewart, R.R., 1990, Joint P and P-SV inversion: CREWES Research Report, **2**, 112-115.